WILEY | Hindawi

Review Article

Directed Energy Deposition via Artificial Intelligence-Enabled Approaches

Utkarsh Chadha[1], Senthil Kumaran Selvaraj[1], Aakrit Sharma Lamsal[2], Yashwanth Maddini,[1] Abhishek Krishna Ravinuthala[1], Bhawana Choudhary[2], Anirudh Mishra[2], Deepesh Padala[3], Shashank M[3], Vedang Lahoti[1], Addisalem Adefris[4], and Dhanalakshmi S[5]

[1]Department of Manufacturing Engineering, School of Mechanical Engineering (SMEC), Vellore Institute of Technology (VIT), Vellore 632014, Tamil Nadu, India
[2]School of Computer Science and Engineering (SCOPE), Vellore Institute of Technology (VIT), Vellore 632014, Tamil Nadu, India
[3]School of Electronics Engineering (SENSE), Vellore Institute of Technology, Vellore 632014, Tamil Nadu, India
[4]School of Mechanical and Automotive Engineering, College of Engineering and Technology, Dilla University, P.O. Box 419, Dilla, Ethiopia
[5]Combat Vehicles Research & Development Establishment (CVRDE), Defence Research & Development Organization (DRDO), Ministry of Defence, Government of India, Avadi, Chennai 600054, Tamil Nadu, India

Correspondence should be addressed to Senthil Kumaran Selvaraj; senthilkumaranselvaraj82@gmail.com and Addisalem Adefris; addisalem@du.edu.et

Additive manufacturing (AM) has been gaining pace, replacing traditional manufacturing methods. Moreover, artificial intelligence and machine learning implementation has increased for further applications and advancements. This review extensively follows all the research work and the contemporary signs of progress in the directed energy deposition (DED) process. All types of DED systems, feed materials, energy sources, and shielding gases used in this process are also analyzed in detail. Implementing artificial intelligence (AI) in the DED process to make the process less human-dependent and control the complicated aspects has been rigorously reviewed. Various AI techniques like neural networks, gradient boosted decision trees, support vector machines, and Gaussian process techniques can achieve the desired aim. These models implemented in the DED process have been trained for high-precision products and superior quality monitoring.

1. Introduction

Artificial intelligence (AI) is a branch of computer science that deals with self-learning mathematical models. For example, weather prediction systems predict weather using AI based on various parameters. Similarly, artificial intelligence has been beneficial in the field of mechanical engineering. This review will rigorously explain that artificial intelligence has made the process of development in the DED process more effortless. It has successfully achieved various goals, including modeling the correlation between the microstructure of alloys and their properties, i.e., with the help of microstructural characteristics like volume fraction and thickness of phase to predict its tensile properties like tensile strength, yield strength, and so on. Experiments can be carried on these alloys more effectively with the properties of the alloys predicted using AI. We have studied a few techniques used in various stages of the DED process, including prediction of single clad geometry, modeling correlation between properties and microstructure of elements, and predicting tensile properties of alloys formed using DED. Using some neural networks and a proper dataset, a

good model can be built to predict temperatures with higher accuracy and precision, leading to an even more efficient deposition technology, which will help build complex and unique parts, especially in biomedical and aerospace industries. We studied how various AI techniques like NN, SVM, GP, GBT, and so on have helped achieve various goals, and we have tried to present an overview of all the techniques [1, 2].

Directed energy deposition (DED) is defined as an additive manufacturing process in which a focused energy source, such as laser arc, electron, or laser beam, melts a material as a nozzle is depositing them [3, 4].

A typical setup of all the components is shown in Figure 1. As seen, the feedstock delivers material (wire or powder) to the deposition point where it is melted by concentrating a laser or an electron beam.

Like many similar additive manufacturing processes, the DED method involves a feeder which directs the feedstock through a heat source to form a weld pool in the presence of a controlled environment such as a vacuum or an inert gas. The feedstock is either a metal wire or powder that deposits on the target object's surface when melted. As shown in Figure 2, there are three widely used heat sources in the DED process [5]. They are electron beam, electric arc or plasma, and laser. In the directed energy deposition process, the heat source is generally focused on the feedstock at the point where metal deposition occurs. G-Code controls the nozzle of the gun or tool in such a way that it follows a specific tool path around the object [6, 7]. The melt pool formed is directed along the tool path by carefully controlling the feed material and the heat source.

2. Understanding Directed Energy Deposition

Figure 3 shows a brief description of how the DED process is generally carried out. The process starts at the point where the material is injected in the form of a wire or powder and completes at the point where all the layers of the material are deposited on the substrate [8]. One must be careful about the residual stresses formed by the enormous magnitude of the thermal gradients created in the heat-affected zone. This results in final products with lesser strength due to the distortion of the grain structure. To reduce these thermal-induced stresses, complex heat treatment processes might be necessary [9, 10]. Due to this reason, the printing process might sometimes be interrupted. Thus, to avoid such circumstances, the printing process must be closely monitored at all times.

The print speed is one of the essential aspects of the DED process. The wire-based DED processes have lower resolution compared to powder-based DED processes. Powder DED processes maintain lower speeds and tend to produce products with higher resolution. Wire-based systems are generally used to create large parts with low printing costs. This is achieved by using low-cost feed materials and higher print speeds. To get higher resolutions and lesser material waste, powder processes can get a near net shape [10]. However, powder processes are relatively expensive compared to the wired processes. We get a near net shape with a much lesser resolution, limited geometric variety, and higher costs for post-processing using wired processes.

As already mentioned in Figure 4, the DED process is conducted in the presence of a vacuum or an inert gas (shielding gas) in order to prevent the weld pool from oxidizing [10, 11]. Reactive metals such as titanium (and its alloys), tungsten, and niobium are some of the most used feed materials used in the DED process. These metals tend to oxidize if there is no shielding gas or vacuum around them. Table 1 shows the pros and cons of these shielding mediums.

Oxidation reactions that might occur during the process:

$$Ti_{(s)} + O_{2(g)} \longrightarrow TiO_2 \qquad (1)$$

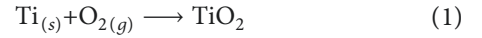$$2W_{(S)} + 3O_{2(g)} \longrightarrow 2WO_3 \qquad (2)$$

Table 2 provides a deep insight and comparison of the additive manufacturing processes on various parameters.

There are many pros as well as some cons of using the directed energy deposition process. One of the main advantages of using this process is that it can be used for various metals, polymers, and ceramics. All the other additive manufacturing processes are usually confined to using metals as the feed material. Many industrial sectors often use this process to repair their existing parts by which they can reduce repairing or replacing costs. The laser or electron beam takes very minimal time to melt the material. Hence, this process has a relatively higher deposition rate when compared to other additive manufacturing techniques. Therefore, the build rate is also high. The nature of the materials used as the feed is selected to cool faster to form round bead-like structures. This makes sure that the parts created are more robust and denser. Also, the precision rate is high, so that there is rarely any need for post-processing or texture enhancements [13]. The DED process makes it convenient for us to change the material whenever needed to make different parts. This is one of the desirable and essential qualities that other additive manufacturing processes do not possess. This process produces near net shape products, and hence the material wastage is low.

Moreover, finally, the DED process can produce very complex objects and through traditional manufacturing processes. This process is also better at making more oversized products when compared to similar processes. This method also has some disadvantages that are to be noted to avoid any manufacturing issues. One such major disadvantage is that the products made by this process have a relatively poorer surface finish than those from other additive manufacturing methods [3]. This is because wire-based DED systems tend to have higher speeds which reduce the resolution of the product. Also, premium features such as overhangs and interior customizing are not possible as support structures are not possible in the DED process. Moreover, finally, the equipment used in this process, such as the shielding systems, energy sources like laser and electron beams, and material feeding systems, is costly, and great care and effort should be taken to manage them.

2.1. Applications of DED. DED is used to fabricate parts but is specially used to add material to existing products or repair. In general, the DED applications come under three
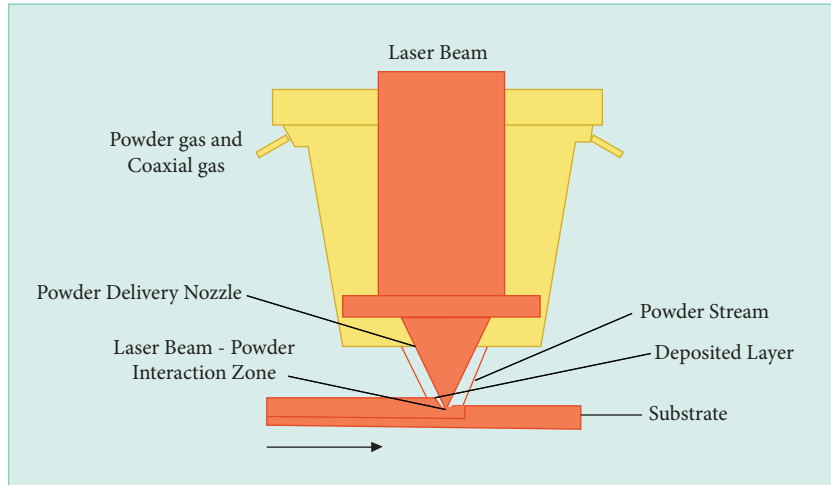
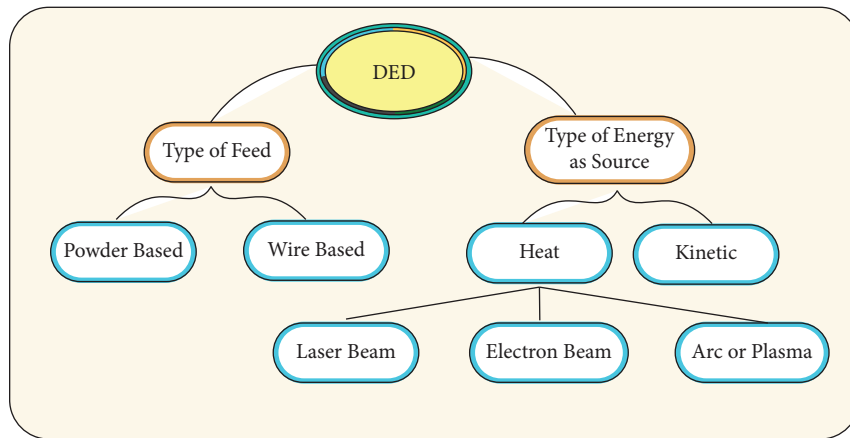Figure 1: DED process setup.

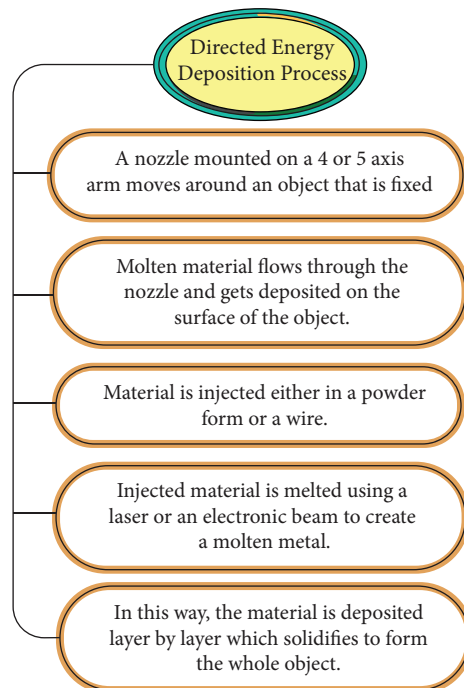

Figure 2: DED classification.
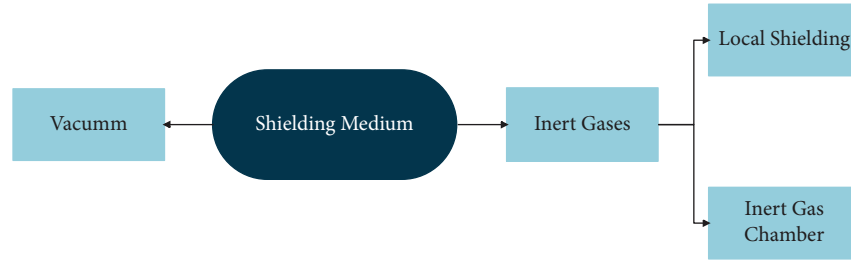

Figure 3: DED process flowchart.

FIGURE 4: Shielding medium.

TABLE 1: Pros and cons involving the use of these shielding mediums.

Pros/cons	Vacuum chamber	Inert chamber	Local shielding	Ref.
Pros	(i) It provides the highest quality environment.	(i) It provides the highest quality environment.	(i) There are some quality compromises which is acceptable.	[10]
Cons	(i) It requires a heavy and expensive reinforced chamber to withstand vacuum forces. (ii) Elements in the melt pool evaporate because of the low-pressure environment.	(i) It is costly and time consuming to fill the whole chamber with inert gas.	(i) It is pretty expensive because of its enclosed environment. (ii) It provides less consistency and atmosphere purity.	[10]

categories (Figure 5). They are near net shape parts, feature additions, and repair. DED is primarily used in manufacturing near net shape parts such as airplane and marine-related parts, saving a lot of time and money. DED can thus produce complex shapes while reducing material wastage. DED can also be used to add some additional features to pre-existing objects. DED uses industrial robots and software tools for the same. It is introduced to add layers to surfaces by using a cladding process with the help of robots. Adding features to objects increases the value of the product. DED makes sure that the machining time is reduced while the only disadvantage being an expensive process. Also, bonding of dissimilar metals is possible by changing the feedstock during printing. A lot more research needs to be done to increase this feature addition process [3, 14]. Finally, DED is used in many industrial sectors to repair existing equipment. A repairing process that was previously done manually got much easier with the help of DED. DED does component repairs often extending the life of the part. It also simplifies the process by reducing the lead time.

2.2. Types of DED Processes concerning Energy Sources

2.2.1. Electron Beam Directed Energy Deposition. Most of the customers choose DED processes to manufacture more significant parts because the DED process has a high deposition rate compared to other additive manufacturing processes. In the DED process, there is a feature addition method that helps to bond two dissimilar metals.

The DED process is subdivided into three categories: electronic beam, laser, and plasma or electric arc. The electron beam additive manufacturing (EBAM) process uses a wire feeder to feed metal wire which directs into an electronic beam to perform on substrate pool. Electron beam gun controls the material and substrate when power is transferred to material [13, 14]. The power values in DED vary with deposition rate, material, and geometry. Most of the time, the power values range from 4 to 20 kw. The EBAM process can be controlled using CAD software to change machine path and axis of tools. This total operation is performed in the vacuum chamber to prevent oxidation. EBAM produces near net shape parts because of its layer-by-layer deposition and is faster than traditional manufacturing methods. This process is used to create parts or components for the aerospace industry as it creates final geometry to components [15, 16]. EBAM works for hours to produce large parts and reduce material wastage. DED works in such a way to get flexible designs. Figure 6 summarizes the characteristics of an EBAM process.

2.2.2. Laser Directed Energy Deposition. The laser directed energy deposition (LDED) process is used to achieve small parts with high resolution, and it does not require any vacuum environment as EBAM. This process comes under powder bed fusion which gives high-resolution parts and maintains low speed [13, 17]. In the powder bed fusion process, parts are built by powdered metal particles that are melted and combined using a laser energy source. Laser DED uses inert gas for shielding and creates finer microstructures.

The main drawback of the laser DED process is that this process requires inert gas for shielding, and manipulation of energy sources also occurs. During building large-scale components, there is a possibility of getting spot sizes [14, 15]. Significant characteristics of the LDED process are summarized in Figure 7.

2.2.3. Arc Directed Energy Deposition. Arc directed energy deposition (ADED) produces or builds more significant parts than the other two DED processes. This is by far the

TABLE 2: Additive manufacturing processes (comparisons).

| Process type	Powder bed fusion	Directed energy deposition	Material extrusion	VAT photopolymerization	Material jetting	Ref
Brief description	Thermal energy selectively fuses regions of a powder bed.	Focused thermal energy is used to fuse materials by melting as the material is being deposited.	Material is selectively dispensed through a nozzle.	Liquid photopolymer in a VAT is selectively cured by light activation.	Droplets of build material are selectively deposited.	[12]
Related technologies	Electron beam melting (EBM), selective laser sintering (SLS), selective heat sintering (SHS), direct metal laser sintering (DMLS)	Laser metal deposition (LMD)	Fused deposition melting (FDM)	Stereolithography (SLA), digital light processing (DLP)	Multi-jet modeling (MJM)	[12]
Materials	Metals, polymers	Metals, polymers, and ceramics	Typically polymer-based	Photopolymer	Polymers, waxes	[12]
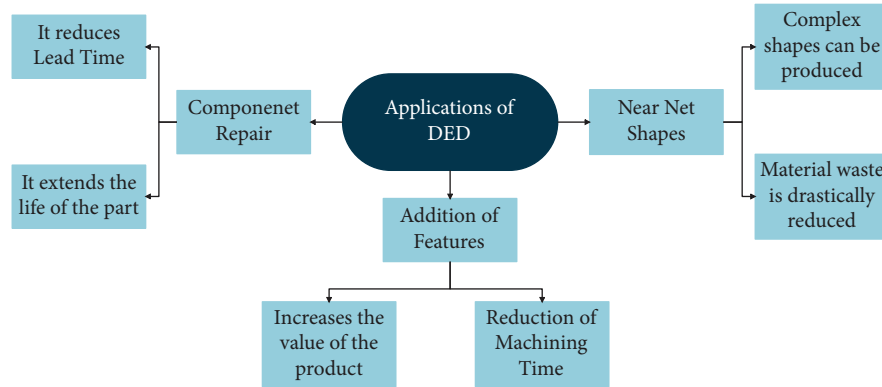
FIGURE 5: Applications of DED.

most commonly available DED method in the market. The arc DED process is used in many industries because it is less expensive than other DED processes [16, 17]. Mainly steel alloys are used to create near net shape parts with high power.

However, there are few drawbacks to the arc DED process. One of the major drawbacks is that the deposition rate is considerably low compared to other DED processes. High deposition rates can be reached with higher traveling speeds under a large volume of shielding gases. Shielding gases used in this process are pure inert gases such as argon which are highly expensive and potentially hazardous [13, 15–17]. All the significant characteristics of an ADED process are listed out as a flowchart in Figure 8.

3. Types of Feed Materials Used in DED

Feed materials are the primary sources for any additive manufacturing process. Feed materials are of two types in the DED (directed energy deposition) process: wire and powder. The selection of suitable feed material is essential to determine various process parameters like viscosity, thermal conductivity, or the coefficient of expansion, and it depends upon the desired features, complexity, and geometry of the final component.

Technology is advancing daily with research searching for new and efficient feed materials that can be used in additive manufacturing processes. While metals and some alloys were the only feed materials used in the primitive stages of DED, a broad spectrum of materials are currently being used in the additive manufacturing industry [13]. Unconventional materials such as superalloys, polymers, nanomaterials, biomaterials, or even bio-waste materials have proven to be suitable replacements for conventional metals and alloys [18–25]. Even though not ready to be used at an industrial scale, recent research on these new materials has shown promising results about using them for mass production in the future.

3.1. Pure Metals. Most of the metals in their pure form have limited applications and very few desirable properties. This is one of the main reasons why pure metals are rarely used for mainstream manufacturing. When combined with other metals, these metals bring out unique properties used in many industrial applications. Even after all these, some of the metals are being used in 3D printing for the sake of research. Some of those metals are listed and briefly discussed below. Table 3 provides a comparison of the pure metal feed materials in the DED process.
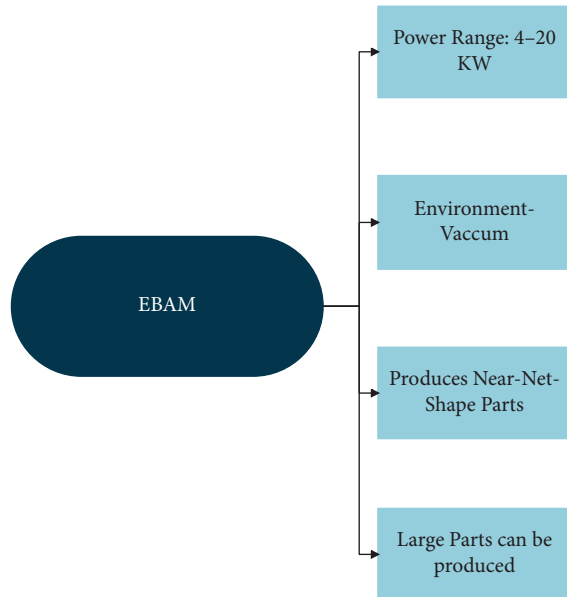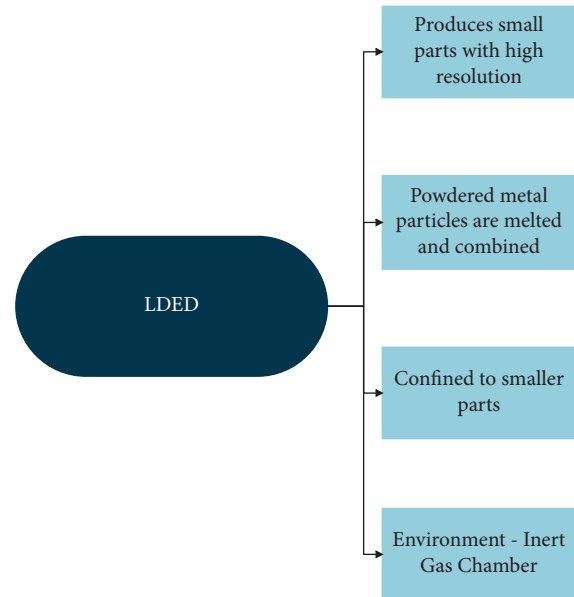
FIGURE 6: Characteristics of EBAM process.

FIGURE 7: Characteristics of LDED process.

3.1.1. Copper. Many aviation and marine industries manufacture heat exchangers, induction coils, or heat sinks for different mechanisms. The DED process allows printing of these products with 99.99% pure copper as the feed material. Copper is considered one of the best metals used for manufacturing such components because it has an exceptional thermal and electrical conducting capacity. Also, it has an excellent heat-retaining capacity and is also said to have anti-bacterial properties. Recent research has shown that the average micro-hardness values obtained by the LDED process are more significant than ordinary Cu samples. One such research is the experiment done by Yadav et al., where they created a block of pure copper by using a 2 kW LDED system [26]. The average micro-hardness value they obtained was 77 ± 3.5 HV0.98 N, which is greater than the average micro-hardness value of copper, which is 57 HV [27]. The results have shown that pure Cu components made using the LDED process have more refined grain structures and better hardness values.

3.1.2. Tungsten. Another metal that is widely used in many industries is tungsten. While tungsten is not directly used in its pure form, it is made into tungsten carbide, a hard material for cutting wood or metals, refining metals, and drilling [28]. Tungsten has many desirable qualities, such as excellent corrosion resistance, low vapor pressure, high thermal conductivity, high melting point, and higher density. This makes it suitable to be used in aerospace and space technologies and nuclear systems. Although fabrication of tungsten is done by using powder bed fusion or spark plasma sintering, recent research studies have shown that DED can also be a suitable process to fabricate pure tungsten. The methods mentioned above are usually time consuming and cannot produce complex geometries [30]. According to Jeong et al., fabricating tungsten through the DED process can solve both problems simultaneously. By the end of their
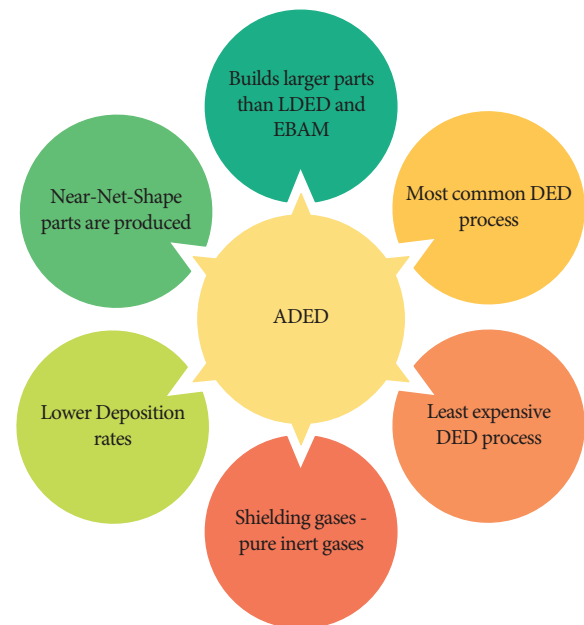
FIGURE 8: Characteristics of an ADED process.

experiment, they could print a pure tungsten structure over 100 mm size, density up to 19.0 g/cm^2, and up to 3.9 GPa hardness. Also, it is concluded that the oxygen level should be less than 300 ppm in the tungsten powder to avoid any oxidation due to the repeated melting and solidification process [29].

3.2. Metal Alloys. Table 4 shows the various metallic alloys as feed materials which are used in the DED process.

3.2.1. Hastelloy-X. Jinoop et al. studied that laser addition manufacturing using directed energy deposition (LAM-DED) is an excellent process to create complex Hastelloy-X

TABLE 3: Types of feed materials (pure metals).

S.no	Materials	Properties	Exploitation on DED	Applications	References
1	Copper	High thermal and electrical conducting capacity, high heat-retaining capacity, and anti-bacterial properties.	LDED	Heat exchangers, induction coils, or heat sinks	[26, 27]
2	Tungsten	Excellent corrosion resistance, low vapor pressure, high thermal conductivity, high melting point, and higher density.	Powder bed fusion, plasma laser sintering, LDED	Wood and metal cutting, drilling, machining, aerospace and space industries, nuclear systems	[28, 29]

TABLE 4: Types of feed materials (metal alloys).

S.no	Materials	Properties	Exploitation on DED	Applications	References
1	Hastelloy-X (nickel-chromium iron-molybdenum)	High mechanical strength, high yield strength, high ductility, high resistance.	LAM-DED	Gas turbine engines, heat exchangers and heat shielding, etc.	[31]
2	Nickel-based superalloy Inconel 718	High tensile and impact strength, good resistance to corrosion and oxidation.	LAM-DED	Jet engines and gas turbines, etc.	[32]
3	Titanium-molybdenum (Ti-15Mo)	Excellent corrosion resistance, hardness, and fatigue.	EBAM-DED	Bioimplants and aerospace industries.	[33]
4	Other titanium alloys	High tensile and toughness.	EBAM-DED	Military, aircraft, spacecraft, etc.	[34]
5	Stainless steel (300 series)	Resistance to corrosion, high strength at high temperature.	EBAM-DED	Plates, sheets, pipes, tube, and fits	[35]
6	Zirconium alloys (Zircaloy)	High hardness, ductility, corrosion resistance.	EBAM-DED	Nuclear technology, water reactor, etc.	[36]
7	4043 aluminum alloy	Good corrosion resistance.	EBAM-DED	Welding and brazing, etc.	[37]

(Hast-X) components on weld pool. Hastelloy-X is used in many engineering applications, especially in gas turbines, heat exchangers, and shields. All these applications are made of Hastelloy-X because of their high resistance and stress corrosion with high strength. An inert gas such as argon has been used for powder feeding. Similarly, laser addition manufacturing uses powder bed fusion (LAM-PBF) to melt Hastelloy-X on the powder bed. Samples built using the LAM-DED process have higher ultimate strength and yield strength than compared to conventional processes. However, it is lower compared to LAM-PBF. Components built using LAM-DED have higher ductility than components built using LAM-PBF. Most complex Hast-X components are being built using LAM-DED because these samples are used for high-temperature applications [31].

3.2.2. Nickel-Based Superalloy Inconel 718. Careri et al. showed that additive manufacturing is the best method to produce complex parts in various automotive, aerospace, and medical industries. Manufacturing parts produced by additive manufacturing processes are more flexible to create near net shape parts. Nickel-based superalloy Inconel 718 is taken in powder with sizes varying from 45 to 106 μm. Inconel 718 is used in nuclear reactors and gas turbine engines because of its high tensile and impact strength. It has good resistance to corrosion and oxidation. The manufacturing process followed by the machining process shows excellent machinability due to the high ductility of Inconel 718 [32].

3.2.3. Titanium-Molybdenum (Ti-15Mo). Titanium-molybdenum (Ti-15Mo) is also called a biomedical alloy since it is used to build biomedical implants, especially orthopedic and dental implants. Laser deposition is used to deposit metal powder on the substrate. Because of its fabulous process parameters, Ti-15Mo is used to build biocompatible implants. The chemical composition of Ti in the deposition part is $85.02 \pm 2.44\%$, and Mo is $14.98 \pm 2.58\%$. Ti alloys are the best alloys for biomedical applications. Two types of Ti alloys are used for biomedical implants: α-type Ti and $\alpha + \beta$ type. Ti-15Mo is used for biocompatible implants because of its excellent corrosion resistance, hardness, and fatigue. Ti-15Mo is quite feasible for bioimplants because of its properties. Similarly, there are some applications used in the aerospace industry. Some advanced research works focus on Ti-15M to learn its applications in biomedical industries [33].

3.2.4. Other Titanium alloys. Compared to the conventional process, manufacturing near net shape (NNS) parts using metal additive manufacturing is more suitable. Near net shape components are built using the conventional process which has various disadvantages such as removing a large amount of material and high cost. Ti alloys in the form of wire and powder have been used to produce NNS components. Ti alloys have high corrosion resistance and can withstand high temperatures. Alloys such as Ti-6Al-4V and Ti-6Al-6V-2Sn are used in the military, aircraft, and spacecraft because of their high tensile strength and

toughness. Metal additive manufacturing is the best method to build NNS because it is more cost-efficient and less costly than conventional manufacturing. For Ti alloys, powder bed fusion is the best way to manufacture components [34].

3.3. Polymers

3.3.1. Polymethyl Methacrylate (PMMA). PMMA is a transparent polymer used as a substitute for standard glass. It is shatterproof and a very rigid thermoplastic material [38]. PMMA is highly resistant to UV light or harsh weather conditions. It has higher chemical resistance when compared to other transparent polymers. It is also highly resistant to scratches. PMMA is mainly used in the biomedical industry to make bone implants, bone types of cement, and drug delivery systems. It is also used to make dental implants where it is substituted for dental roots [39]. Mitsouras et al. described that 3D printed endoprostheses used for the palliative care of patients were created using selective laser sintering and directed energy deposition of PMMA and were sterilized using γ radiations [40]. When these materials are observed for 486 days (about one and a half years), the functional outcome was good in 70% of the patients and was fair in the remaining patients.

3.3.2. Polyether Ether Ketone (PEEK). PEEK is a semi-crystalline thermoplastic with high performance. PEEK is used in the medical industry as supporting parts of endoscopes, dialyzers, and dental instruments. This is mainly because of its high heat and electrical resistance. It is used in the aircraft industry to replace parts made of aluminum [41]. PEEK has a high melting point, and thus it can withstand high temperatures. Therefore, it is used in critical engine parts in aircraft. It also has similar applications in the automobile industry [42]. Rinaldi et al. fabricated nanosat structures using PEEK as the feed material and FDM process. They described that the part was made, but there were many thermal-related issues in part. Despite these hurdles, they achieved an acceptable value of thermal conductivity (5 w/mK). Thermal conductivity needs to be within the acceptable values to ensure a minimal number of hotspots forming on the surface. Also, it was understood that the temperature should not exceed the polymer glass transition temperature to ensure no drop in the mechanical properties [43].

3.3.3. Acrylonitrile Butadiene Styrene (ABS). ABS is majorly used in automotive applications to reduce weight by replacing conventional metallic parts. Dashboard parts and bumper parts are some examples. ABS has high impact strength and heat resistance. This makes it very apt to be used in pipe materials, and fittings can withstand earth loads and high temperatures. ABS is used in many structural applications due to its stain resistance and stability over time [44]. ABS fused with MOF (metal-organic framework) materials can also be extensively used for gas storing, filtering, sensing, and catalysis, as described by Bible et al. in

their research. They were able to fabricate an ABS-MOF composite without any visible defects successfully. Bible et al. created two ABS-MOF materials ABS-ZIF-8 and ABS-HKUST-1 and tried adsorbing N2 and found that the printed ABS-HKUST-1 adsorbs more N2 (70) than ABS-ZIF-8 (55) [45].

3.3.4. Polypropylene (PP). Polypropylene is one of the cheapest crystalline thermoplastics available in the market. PP is produced when a propene monomer is polymerized. PP is extensively used in the packaging industry due to its excellent barrier properties and low cost. This is used in food packaging because of its low moisture-vapor transmission and exceptional optical clarity. It is also used as battery cases and instrumental panels in the automotive industry. In the medical industry, polypropylene is used in making disposable syringes, Petri dishes, diagnostic devices, etc. due to its high bacterial and thermal resistance [46]. Polypropylene is also used as water filter nets and feed spacers to treat sewage and wastewater in wastewater treatment plants. Tan et al. successfully created polypropylene net-like structures through SLS (selective laser sintering) to measure the effectiveness of polypropylene as a suitable material for feed spacers. It was found from the results that Young's modulus and the ultimate strength are directly proportional to the amount of energy density used [47]. They have also concluded that raw PP powder is not suitable to be 3D printed with the process parameters they have taken, and much research about the ideal process parameters needs to be conducted.

Table 5 shows all the polymer-based feed materials for DED process.

3.4. Ceramics

The additive manufacturing (AM) process is appropriate to shape different ceramic parts. There are two types of AM processes: direct and indirect. The indirect AM process is used to produce appropriate components, and direct AM produces large parts. The AM process can produce pore and crack-free ceramic parts. In the traditional DED process, ceramic powder has been used to melt and solidifies on the substrate. In the hybrid fused DED process, the wire has been used to build parts [49]. Ceramics are widely used for dental applications. Ceramics with high chemical stability, biocompatibility, aesthetic, and mechanical properties replace or restore damaged teeth.AM is used for mass production, and it is the least expensive [50].

3.4.1. Alumina. Alumina is one of the widely used ceramic materials. It is well known for excellent electric insulation and is highly resistant to corrosion. It has a wide range of applications such as automotive sensors, dental implants, and electronics [51].

3.4.2. Zirconia. Zirconia ceramic is the most studied and more robust material in ceramics. It provides unique properties which provide high demand to its applications. It offers high toughness, high strength, and corrosion

TABLE 5: Types of feed materials (polymers).

S.no	Materials	Properties	Exploitation on DED	Applications	References
1	Polymethyl methacrylate (PMMA)	Shatterproof, rigid, UV and harsh weather-resistant, highly resistant to scratches	Selective laser sintering (SLS), DED	Biomedical industry, automotive and transportation industries, furniture industry	[38–40]
2	Polyether ether ketone (PEEK)	High heat and electrical resistance and can withstand high temperatures	FDM (fused deposition method)	Medical industry, aircraft, and automotive industries	[42, 43]
3	Acrylonitrile butadiene styrene (ABS)	High impact strength and heat resistance, high strain resistance, and stability over time.	DED	The automotive industry, pipes and fittings, structural applications	[44, 45]
4	Polypropylene (PP)	Excellent barrier properties, low cost, low moisture-vapor transmission, exceptional optical clarity, high bacterial and thermal resistance	SLS	The packaging industry, automotive industry, medical industry	[46, 47]
5	Polylactic acid (PLA)	Biobased, biodegradable, biocompatible, compostable, non-toxic polymer	DED	The packaging industry, health and medical industry, structural applications	[48]

TABLE 6: Types of feed materials (ceramics).

S.no	Materials	Properties	Exploitation on DED	Applications	References
1	Alumina	Electric insulation and resistant to corrosion	LAM-DED	Automotive sensors, dental implants, electronics, etc.	[51]
2	Zirconia	Toughness, high strength, and corrosion resistance	LAM-DED	Dental crowns, insulators, rollers, pistons, etc.	[52]
3	Magnesium aluminate spinel	High strength	LAM-DED	Bulletproof glass, aerospace, and defence.	[53]

resistance. Widely used applications include pistons, rollers, insulators, bushings, dental crowns, and more. It has been used for dental crowns because of its high strength and longevity [52].

3.4.3. Magnesium Aluminate Spinel. Laser directed energy deposition is feasible to fabricate magnesium aluminate spinel (MAS) ceramic parts. Because it is costly to manufacture using the traditional method [51], MAS is a high-strength ceramic used for bulletproof glass applications. These applications are used in industries such as aerospace and defense [53].

Table 6 compares the feed materials based on ceramics, which are used in the DED process.

4. Implementation of Computational/AI Models in DED

Additive manufacturing was founded with the Internet. Hence, it has always had the networking and communication capabilities that its traditional counterparts did not. Because AM is a digital process, it may produce large datasets throughout a build. The value of additive manufacturing resides in creating components that are performance-optimized and can only be created using AM technologies. AM aids in reducing assembly and, all with it, touch labor by allowing components that would normally be formed of various pieces to be created in a single piece. This information or digital input may then be utilized to maximize the physical output using machine learning and artificial intelligence. We expect that this translates into greater productivity, higher production, and the capacity to seal the quality control loop rather than depending on expensive inspection techniques.

Artificial intelligence can make additive manufacturing processes less tedious than they presently are as well as increase the precision of the process. Computer vision may be used to analyze current physical items to reverse engineer them and create a new, enhanced product design based on the current model. This can help to speed product development and improve processes while also reducing the time taken to produce new items.

Machine learning and artificial intelligence are indeed assisting in generative design, in which a software program generates design models automatically depending on the needs and restrictions stated by the technical department. This allows design engineers to investigate novel design solutions to address the most challenging problems. These designs may be swiftly turned into tangible prototypes or operational models by utilizing additive manufacturing processes.

Product development is typically a time-consuming operation that necessitates the investigation of multiple viable design possibilities before arriving at a final solution. With AI-driven generative design, this approach of
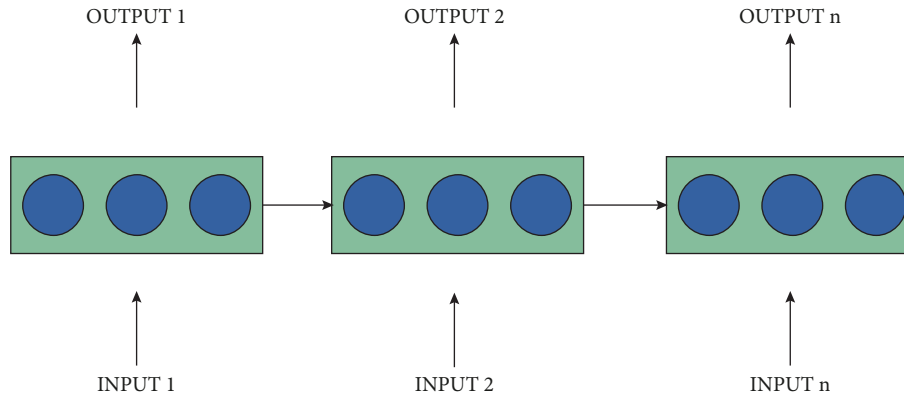
FIGURE 9: RNN chain.

iteratively evaluating multiple concepts may be significantly amplified. Design teams may use additive manufacturing techniques to undertake fast prototyping to transform designs into 3D models for evaluation and approval for large-scale production in an unparalleled short time frame, increasing design productivity.

The application of AI in DED also helps to improve the quality of the product by designing products with good quality standards paired with consumer-friendly functionality. This assures greater client satisfaction, which may result in increased profits and revenue. Following the implementation of IoT in production, the advent of AI applications in DED will most likely be the industry's upcoming revolutionary surge. AI-driven additive manufacturing can be the major technique of making new models in the future if advances in disciplines such as precision automation and machine learning continue.

Although machine learning is already used in creating AM products, the interconnections have not yet been completely realized. We are witnessing data, which could be from multi-dimensional data or existing sources, advising algorithms that can alert consumers of chances for improvement. Machine learning is now strongly a part of the progress of AM, from designing materials to powder feedstocks, through the AM equipment in the form of variables, and eventually with parts.

4.1. Machine Learning (ML) to Predict the Temperature of the Melt Pool.
ML can be used to predict the temperature of the melt pool by looking at other parameters surrounding it. Two such ML algorithms are tested, namely, XGBoost and an LSTM. Both are good at predicting melt pool temperature.

Recurrent neural network (RNN) is a special type of artificial neural network. RNNs in general are capable of remembering and using previous results to predict the next result by sensing patterns in the sequential data given to it. But as the length of these dependencies grow, the traditional RNN starts to have less accurate results. This is because of the vanishing gradient problem [54]. The problem is accentuated in prolonged sequences of data. The gradient decays with each update as it propagates backwards in the data

stream. This causes the backpropagation algorithm to gain more insights from the last data point when compared to the first one; for example, in Figure 9, the RNN will learn more from input n than it will from input 1. This could prove detrimental to the accuracy of the algorithm as it may miss important signs from the earlier stages in the stream of data given to it.

This issue can be remedied using LSTM [55]. LSTMs are special as they are capable of handling long-term dependencies. LSTM neural networks consist of a chain of repeating modules of neural networks too, unlike RNNs. The major difference is that it has a different structure in each module as you can see in Figure 10. The core idea behind LSTM is the cell state, which runs through the entire chain of modules, with only minor linear interaction. It basically helps in the ease of the flow of information. Another huge advantage of the LSTM is the ability to selectively read, write, and forget information [55] which are taken care of by the various operations shown in Figure 10. These help it derive information from the entire dataset without giving any data point preference just because of its position in the sequence. This makes it a very robust algorithm, which can easily recognize sequences, irrespective of the length of the data chain.

Extreme gradient boosting (XGBoost) is a highly scalable algorithm, capable of handling wide range of problems with high accuracy. Benefiting from the automatic parallel computation and customized tree structures, the algorithm is reported to be ten times faster than normal boosting tree algorithms. XGBoost algorithm involves creation of sequential decision trees where each tree is capable of fitting the residual of previous tree. Each tree can be understood as a weak base learner having relatively low predictive accuracy, and combined (as shown in Figure 11), these trees give a boosted performance. Also for the best results, few hyperparameters like the number of trees, maximum depth, learning rate, and minimum child weight of leaves are tuned based on previous research.

The prediction was similar, with a significant variation in the melt pool temperature. LSTM performs slightly better with low variations, but the efficiency is lower when compared to XGBoost. XGBoost is 400 times faster than LSTM in one of the situations in the testing. Their performance is
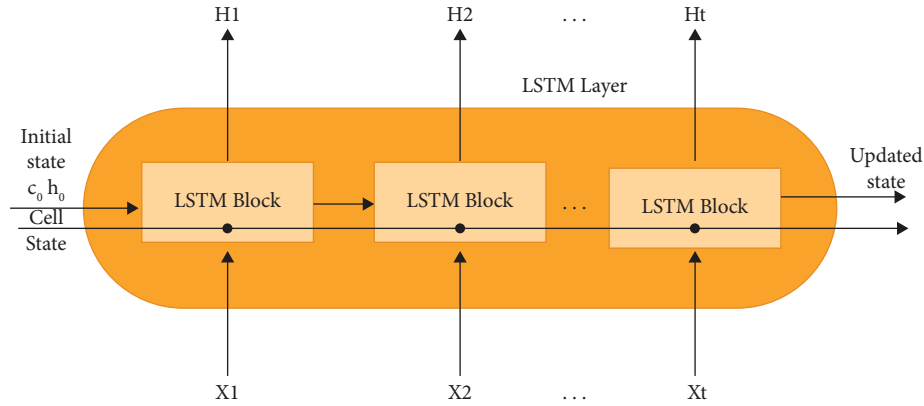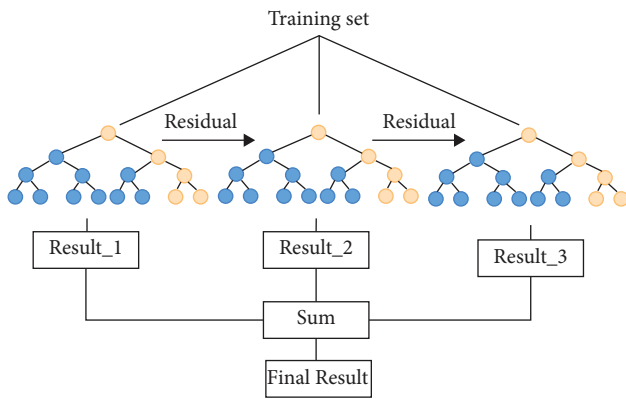
FIGURE 10: Working of LSTM.

FIGURE 11: XGBoost algorithm.

for feature extraction and pattern recognition by the CNN model. Authentic images of the DED process were used for testing the validity of the model. Such a strategy produced convincing results at recognizing patterns in parameters such as scanning speed and laser power in [57].

Convolutional neural networks (CNNs) come under the category of deep learning algorithms specialized for working on images (applications such as segmentation, classification, and object detection). They consist of convolutional layers, maxpool layers, and dense layers. Convolutional layers make use of the convolution operation (i.e., element-wise multiplication) of the image with other tensors known as filters in convolutional layers, whose weights are assigned relevant to the processing to achieve the desired mapping between input and output using the backpropagation algorithm [54]. Since images are heavy on capacity and computation, maxpool layers (Figure 12) work on compressing the image size with minimal loss in important features.

Image tensors being of the form of multi-dimensional tensors have to be flattened out in order to correspond to a single output label after which further linear and non-linear processing is carried out in dense layers on the converted tensor leading to the output label. The thermal images were passed to a deep CNN architecture (Figure 13) for image extraction and classification.

compared with ridge regression, which turned out to be inferior [56].

Some hyperparameters were adjusted for XGBoost, such as learning rate, number of trees, maximum depth, subsample rate, and the minimum child weight. This was done according to the findings from previous experiments [56]. Similarly, for LSTM, some hyperparameters were adjusted, such as mini-batch size, the number of epochs, the learning rate, the sequence length, the number of hidden layers, and the hidden layer size. This was done according to the findings from previous experiments [56].

Data from 24 experiments were used for training the model for the predictive model, and the rest were used for validations and testing. The data consisted of input variables and an output which is the melt pool temperature [56].

4.3. Using a Recurrent Neural Network (RNN) to Predict the Thermal History of the DED Process. An RNN structure (shown in Figure 14) alongside a gated recurrent unit design predicts thermal history in the directed energy deposition process with distinct geometry, laser power, build dimensions, toolpath strategy, scan speed, and toolpath strategy. RNN was the best choice simply because RNNs permit the learning of the data's temporal dependencies without further specifying things. Also, the traditional time series need precise adjustment every simulation. This makes RNN suitable for this kind of particular setup [58].

A stacked recurrent neural network structure with GRU formulation is used in the research. Each GRU cell receives an input feature (x_t) for a particular time step and a hidden state from the time step before this step (h_{t1}). The output is a new hidden state (h_t). The dimension is the number of units

4.2. Using a Convolutional Neural Network (CNN) to Predict Scanning Speed and Laser Power. Identification of additive manufacturing processes is carried out via the application of deep learning. The algorithm employed map supplied input images to corresponding output labels based on the features extracted from the training data passed onto the model. In this case, the input supplied is in the form of thermal images of the time series collected by a camera consisting of various settings of the DED process. These thermal images were used
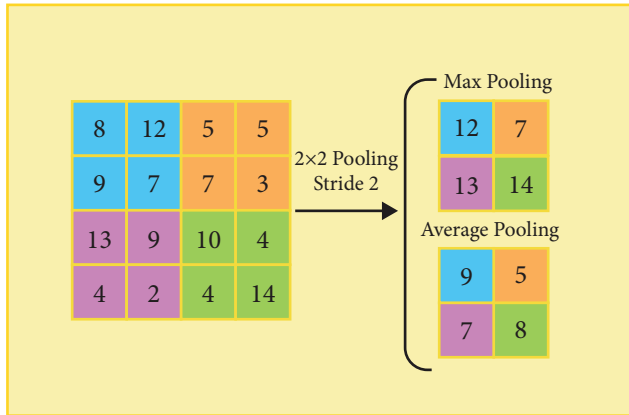
FIGURE 12: Pooling layer functionality.

per GRU cell. With the help of weights and biases, the state connects to other cells [58].

Developed using the Keras deep learning library, the model was built. The Adam optimizer was used, and the MSE function was used to evaluate the costs and results. The data were prepared using GAMMA. GAMMA is an in-house finite element code for thermal analysis [58].

4.4. Finding Surface Cracks Using LSTMs. The laser spot scanning system is designed to produce a multi-mode heat source with various modes with a controlled spatial position and excitation time. Depending on the detection system, combining the LST method with the neural network's short-term neural network (LSTM) (represented in Figure 15), a new process of finding surface cracks was introduced. A post-processing algorithm was developed to extract the feature signal after the LST scan method indicated the split distribution: temperature and temperature gradient. The signal that is to be inserted into the neural network for training went on to predict the crack width. When verification of the reliability of the LSTM neural network was performed, cracks in the actual surface of the LENS variety were predicted. The estimated total error of the LSTM neural network for predicting crack width was observed to be 2.0 μm (and the total error detected was 6.1 μm) of crack with a range ranging from 3–68 μm [59].

The numerical mesh was created for modeling a cracked sample using the ABAQUS software. A periodic thermal source with a square wave pattern was touched on the model's surface using a FORTRAN code [59].

LSTM neural network is used in this project for its ability to analyze sound and text. It has the following layers: an input layer, a recurrent hidden layer containing memory blocks, and an output layer. The memory blocks contain special memory cells that aid in self-connections for storing temporal states and gate units. The flow is controlled with the input gate (it) and the output gate (ot) [59].

The amplitude and heat source radius were finely adjusted. Then, the task was executed to see the thermal response for the cracks having different depths and widths. Lastly, the thermal response with no noise, which was
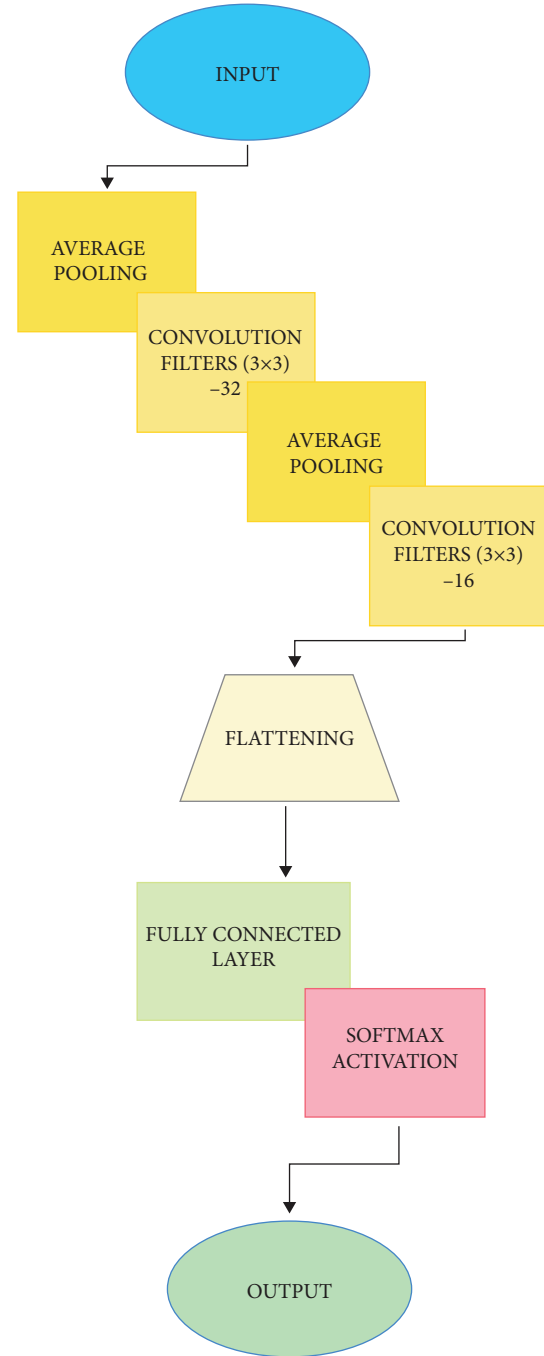
FIGURE 13: CNN architecture [57].

obtained via the experiment, was used to determine the structure of the neural network. The next step was to modify network elements and apply the model to detect artificial cracks [59].

LSTM NN was trained with data gathered from the FEM simulations and artificial crack tests. To obtain (surface) temperature field, numerical replications were used. The surface temp was observed to rise due to our sample's thermal excitation having cracks of varying widths and depths. The temp features required were gathered from the thermal image of the location of the cracks. The data were
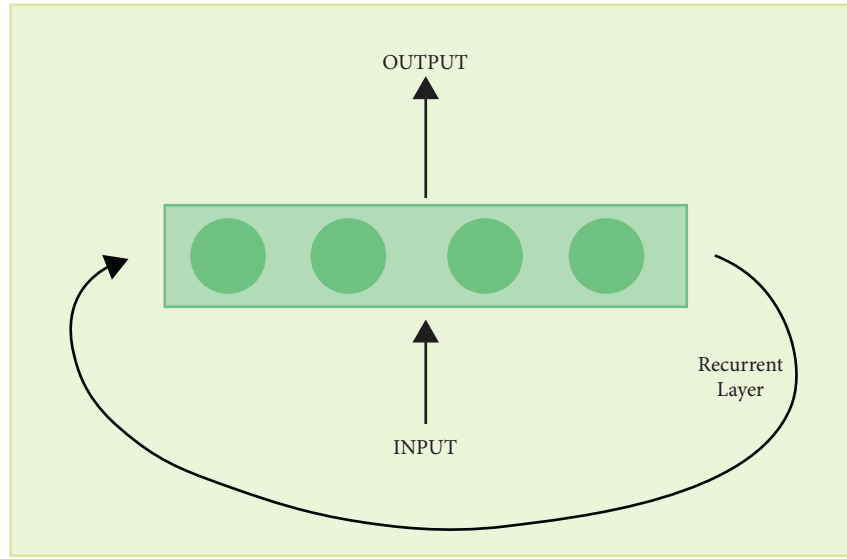
FIGURE 14: Recurrent neural network.
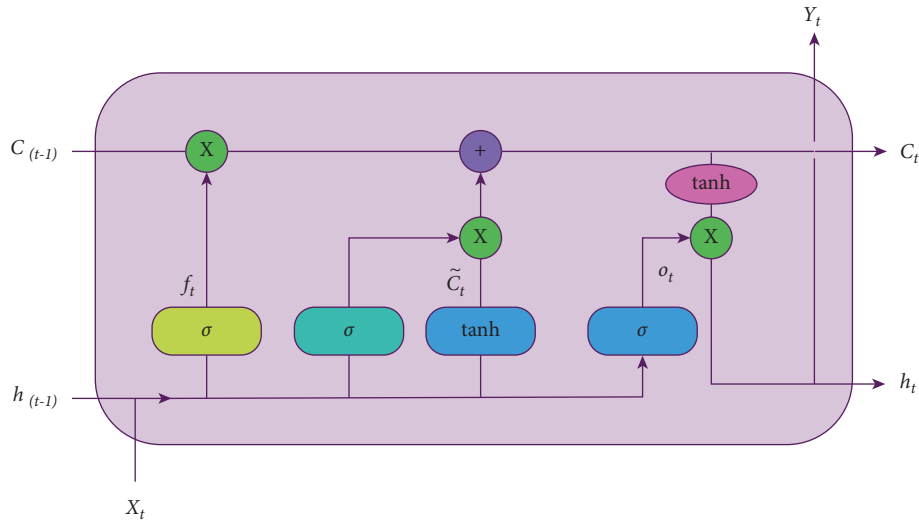
FIGURE 15: An LSTM block.

gathered from three crack widths and depths. The structure has the following layers:

(i) Input layer

(ii) LSTM layer

(iii) Fully connected layer

(iv) Dropout layer

(v) Fully connected layer

(vi) Regression layer [59]

4.5. Prediction of Tear Rates Using ANNs. In another paper, an artificial neural network (ANN) was used to validate and optimize the process and results. Data used were selected and pre-processed. The input parameters were L0 orthogonal array and three input variables, namely, layer thickness (LT), orientation, and temperature. The output consisted of a single variable: wear rate. The neural network had 10 neurons in its hidden layer and was trained using an accelerated gradient descent algorithm with an adaptive learning rate [60]. Gradients were generated using the mean squared loss metric.

4.6. Using ML to Predict the Depositing Height (DH). This implementation was made with laser engineered net shaping (LENS) in mind, as one of its main drawbacks is controlling the DH. This is mainly because of the large number of parameters that affect the process. This is where ML algorithms come in. They can easily predict the DH by parsing all the parameters that affect the DH.

The algorithms tested are the backpropagation and adaptive learning rate and momentum coefficient (BP-AM)

and the LS-SVM (least squares support vector machine). Input specimen comprised of main parameters that affected the DH. Also, the DH (output of the algorithms) of a single track was accumulated with the help of LENS experiments [61].

The BP-AM consists of only one input layer. Since there are three inputs, three nerve cells were also required. The input consists of PFR, laser power, and scanning speed. When the hidden layers were increased to 3 in size, the training time also increased, with the equivalent error for the same training sets. Due to this, the hidden layer was set to consist of only one layer.

The output consisted of one neuron, producing the DH of a single track. The thresholds and weights were initialized using random values in the range of 1 and -1 for BP-AM, while the increment was initialized to 0. The maximum loop time, goal error, momentum factor, and learning rate were optimized as 100,000, 0.01, 0.95, and 0.03, respectively.

The training data were provided, which included the parameters and the results from the experiments. This was acquired before the training of the BP-AM model. The data were normalized [62] before the training was done. After the successful training, this model was tested in the LENS process for predictions [61].

Like the BP-AM model, the LS-SVM model was also facilitated with the normalized training datasets and trained. For the optimization of the model, the MSE value was calculated and used. As for the performance index, MSE and relative error from the predictions were calculated and used [61].

4.7. CNNs to Classify DED Patterns.

DED patterns caused by different types of particles might look similar to the human eye, albeit with subtle differences. It is these differences that a CNN will easily be able to pick up on and categorize which can aid the manufacturing process.

The input layer of the CNN had a size of 28×28 (2D image), and the architecture had two convolution layers. Layer 1 consisted of ten filters of kernel size (6×6), and layer 2 had 20 filters of kernel size (4×4), both with a stride of (1×1) to ensure that the filters were passed over every pixel. These layers helped in feature extraction (edges and shapes). The ReLU activation function was applied to the outputs to introduce non-linearity to the neural network. The output of the convolution layers was reduced by a max-pooling layer of pool size 2×2, which reduced the dimension of the images by 50% on each max-pool operation. After flattening the $20 \times 20 \times 7$ output, 980 values were obtained, which were then passed to a fully connected layer connected to another fully connected layer containing 2000 neurons. To prevent the model from overfitting, a 50% dropout rate was applied; this means that while training, the gradients were applied to only 50% of the neurons at each update. This prevented one set of neurons from dominating the decision-making process [63].

As for the dataset, the authors used 100,000 images, 50,000 of each class. The images were categorized as follows:

(i) 60,000: training

(ii) 20,000: validation

(iii) 20,000: testing

4.8. Using RNNs to Predict Thermal History.

A stacked RNN structure can be used with a GRU design to predict the high dimensional thermal history at a given point. The model was showing an MSE of $2.97e - 5$ after 100 epochs of training. The predictions were further examined for a more extended period and non-trained geometry. In additive manufacturing processes, RNN can make predictions of complicated behavior. The model could be further enhanced by incrementing the number of epochs the model goes through while training and increasing the different types of geometries present in the datasets [58].

The inputs consist of the time step (ht) and a previous time step's hidden state (ht-1). This gave out a new hidden state (ht) as the output. The dimension (hidden state) is equal to the number of units per GRU cell. The hidden state makes a connection to other states using weights and biases. To comprehend the deep-lying correlation in the data, the model uses multiple layers of the GRU structure. To combine the different outputs into one time-series temp output, the fully connected layers were used. Keras library was used to build the model. Adam optimization was used for optimization, and for the evaluation of the model, MSE cost function was considered [58].

The RNN model was trained with various configurations. It involved GRU units (100–500), 1–5 RNN layers, and 1–3 fully connected layers. Reaching the MSE value of $1e - 4$, the model displayed promising results in just 100 epochs and a few layers and units. When increased to 3 stacked GRU layers, the model had only $3.210e - 5$ MSE on training and $3.84e - 5$ on testing with 100 epochs. The training time was observed to be approximately 40 h on Nvidia Quadro P5000 [58].

4.9. Predicting the Correlation between Microstructures Using ANNs.

To explore the effect of microstructure on mechanical properties of Ti-6Al-4V, an alloy, few experiments like forging, heat treatment, and tensile tests at room temperature were done on the alloy. A relational model between microstructure and mechanical properties was documented using an artificial neural network (ANN) where the proposed model took quantitative microstructural characteristics, volume fraction and thickness of phase, and the Feret ratio as input and gave tensile properties like ultimate tensile strength, yield strength, increment, and decrement in the area as the output as shown in Figure 16. ANN techniques are believed to be one of the most effective ways and are enormously used in material science for various tasks like developing intrinsic relationships, predicting mechanical properties, and optimizing processing attributes. In this case, the architecture with a single hidden layer was chosen because these kinds of three-layer neural networks can approximate most of the simple functions given that the hidden layer has the right number of neurons. Had the number of neurons taken in the hidden layer been
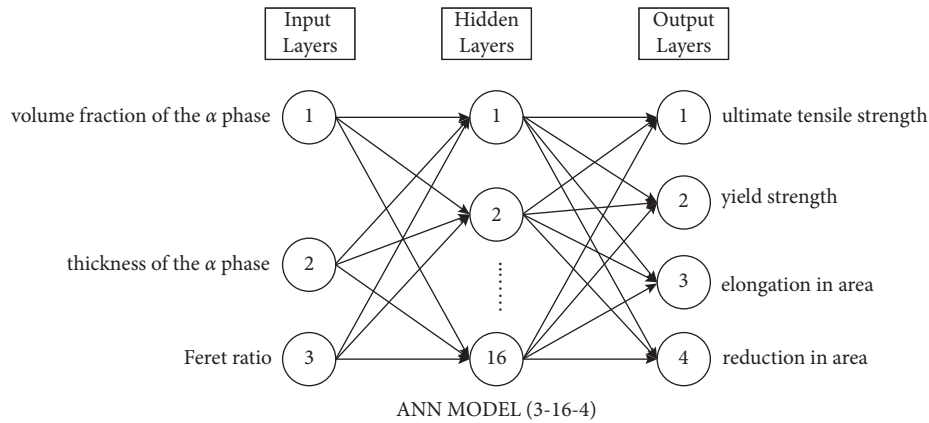
Figure 16: Overview of an ANN model.

less than what was required, then ANN would not have the desired approximating capability, and if they were more than what was required, then the model will get overfit, which is the phenomenon in which the neural network picks up on unwanted variations in the training data, making it seem highly accurate, while performing badly when presented with previously unseen data. Hence, several permutations were processed by a computer program compiled by the authors. Considering the number of neurons in the hidden layer and its effect on the network's performance, the number of neurons was altered from 1 to 20. To avoid overfitting, architectures containing more than 20 neurons in the hidden layer were not tested. Based on these experiments, it was found that the network with 16 hidden layer neurons gave the best output with desired error tolerance. The structure was deduced to be 3–16–4 in the model. The input layer had three nodes: volume fraction of the α phase, the thickness of the α phase, and Feret ratio. Moreover, the output layer had four nodes: ultimate tensile strength, yield strength, elongation, and reduction in area. To train the model more efficiently, input and output data had been scaled to a range of 0.1 to 0.9. There was less than 5% error between the expected and tested values, which showed that the model could predict the necessary relations. The collective impact of characteristic microstructural constraints on the mechanical properties of the alloy had been examined using this model to check the completeness ability of the model. When calculated, all the values of R were more significant than 0.90 and MAPE was 1.22%, which showed that the prediction results were fit for at least 90% of experimental results and that the model could successfully predict the internal relationship between microstructure and mechanical properties of the alloy with operational reliability [64].

Similarly, a model was developed to predict the same alloy's tensile properties using the hybrid ANN and genetic algorithm approach. At first, the ANN was trained and then tested, with the assumption that fitting did not occur. As a result, the authors got an n-variable response surface where variables were microstructural parameters and their composition. The ANN was also explored using virtual experiments to estimate the importance of each input by keeping other input values average. These experiments are then used in conjunction with theory to estimate "loadings" (a set of possible ranges) that unknown pre-factors and exponents for a physically-based equations might take. Then, the GA finds an ideal solution. As the GA is about to meet the solution, the response surfaces produced by both the models, GA and ANN, are compared using the virtual experiment. Then, based on how identical both models are, models closer to theoretical values of the terms and models with minimum scatter between predicted and experimental values are given higher weights. In this way, a physically-based model with predictive capability as an adequately trained ANN model can be produced but with a basis of physically understood strengthening mechanisms. The authors, for achieving the aim, used convolutional neural network (for feature extraction in thermal image data) and ANN approaches (to identify parameter effects) to investigate thermal history images of the build process and process parameter influences in distortion to develop the approach [65].

4.10. Using ML to Predict Single Clad Geometry in DED.

There can be a sequential description of physical events occurring at directed energy decomposition with powder injection. When the laser energy hits the substrate, a significant fraction of its energy is imparted there. The residual energy is distributed among reflection and energizing powder particles, making their path to the substrate. This process can be said alternately as the laser creating a melt pool into which metal powder is injected to build the clad. To better understand this process of directed energy decomposition and cladding, models have been established to predict the outcomes and dynamics of the process. When classified broadly, there are two types of these models: physics-based model and empirical-statistical-based model. The basic physical phenomenon gives analytic results of heat transfer, mass transfer, and continuity under certain sets of assumptions and boundary conditions. However, these models lose predictive power in the face of process variability. The author had devised a method that falls under the empirical-statistical model of data science. Empirical-statistical models address process variability by taking direct

measurements and constructing process maps to predict directly tested behavior. Moreover, even in empirical-statistical models, regression models are the best and most studied form. They are easy to use and have significant value in the practical sense [66].

The dataset used to train this algorithm is a collection of process parameter study data points. The input set comprises powder material (one hot encoded [67]), substrate material (one hot encoded), spot size (mm), power (W), mass flow rate (g/min), travel velocity (mm/min) and the deposition resultants (height (mm), width (mm), and contact angle (deg)). For classification to be performed, the output of interest and aspect ratio (H/W) had to be split into classes before applying the ML techniques. Since the original data were continuous, a target value of 0.5 was chosen, and intervals of increasing distance were formed around that target value, discretizing the data, making it easier for the algorithm to parse. The author developed dataset-wide models based on ML techniques to assess the predictive power of those models. The ML techniques used were neural networks, gradient boosted decision trees, support vector machines, and Gaussian process techniques. Results of all these models were compared to check which one performed the best. With the dataset pre-processed, the application of the previously mentioned machine learning techniques was performed. The neural network architecture used in this study borrows from McGhee and uses what is termed a linear "skip connection" [68] to evade the vanishing gradient problem. The generalized notion is that this set of neurons with only a linear activation function will capture linear artifacts in the data while the non-linear neurons will then capture the non-linear artifacts. McGhee suggests this architecture as a means to increase the effectiveness of NNs on tabular data [66].

Neural network regression exhibited a response plot similar to logarithmic curves inherent in the empirical-statistical models. There was a fair amount of variance still present in the results of the regression model. This indicates a shortcoming in the model when provided with a high variance dataset. However, the success of the model is that it produces a generalization between material and processing conditions. This non-reduction of variance is seen when examining the classification results of the neural network model. The network is only a binary classifier, even though it was subject to multi-class input. The response surface of the GP model indicates a departure from the logarithmic curves of the NN and empirical-statistical models. This departure results in minor variance than those models. This is further supported by the classification results where the GP model is more than simply a binary classifier. The inclusion of more classes yields a better predictive model. The deduction is that the Gaussian inductive prior of the GP model is more informative at a high dimension than the radial basis kernel in this dataset. SVMs, when compared to the NNs, have lower variance and better classification accuracy, even though the SVMs and NNs both entirely overestimate non-optimal clads as classifiers. The gradient boosted decision tree (GBT) model lends credence to its effectiveness on tabular data. The resulting classification distribution closely follows that of the dataset. However, the coefficient of determination, r^2 value, is the lowest of all models examined. This suggests that outliers might be over-penalized by the model, lowering the R^2 value [66].

4.11. Predicting Surface Characteristics in CO2 Laser Micro-Milling.

For predicting the surface characteristics, i.e., depth and surface roughness of plastic composite augmented by glass fiber, an approach using ANN to be applied after CO2 laser milling consisting of layers and neurons has to be developed and optimized. In ANN, there are three types of layers, i.e., input layer, hidden layer, and output layer. Hidden layers are responsible for establishing a connection between the rest of the layers based on learning by the data. Neurons include inputs, weights, a summation function, an activation function, and outputs. The summation equation as given in the below equation finds the total input of the neuron:

$$\text{NET}_i = \sum n_j = 1 w_{ij} x_j + w b_i, \tag{3}$$

where NET_i is a weighted sum of inputs to the ith processing element, wb_i represents the weights of biases between layers, x_j is the output of the jth processing element, w_{ij} represents the weights of the connections between the ith and jth processing elements, i and j are the processing elements, and the number of processing elements in the last layer. It used various network structures like 3-1-3, 3-3-3, 3-6-3, 3-7-3, 3-1-1-3, 3-3-3-3, 3-6-6-3, 3-7-7-3 based on trial-and-error process. The previously mentioned sequences of numbers are the orders of the number of neurons in the layers of the ANN. For the training dataset, many parameters such as the availability of material, cost, and time required for conducting the experiments were considered. The dataset of 60 experiments was considered and assumed to provide the most accurate results in predicting surface roughness using ANN for testing the model. The algorithm chosen to implement was the feed-forward backpropagation algorithm. The approach used log sig transfer function, and evaluation of the model was done based on mean square error (MSE) performance function. The mean prediction error for each network structure was calculated, and based on results, two hidden layers with six nodes in each were found to be the most accurate one, i.e., 3-6-6-3. Hence, it was concluded that the ANN approach using a 3-6-6-3 network structure is the most suitable one [69].

4.12. ANN to Predict the Grain Boundary Tilt Angle While Performing DED with Titanium Alloys.

An ANN model was developed to investigate the connection between grain-boundary tilt angle and three causative factors, i.e., thermal gradient, crystal orientation, and Marangoni effect in DED. Experiments like EBSD, melt pool cross section observation, and grain-boundary tilt angle measurement were performed to extract and train the model. Using these experiments, 50 groups of data were collected to evaluate the ANN model. This model followed a feed-forward neural network with network structure 1-5-10-1, i.e., input and output layer with

one neuron each and two hidden layers with 5 and 10 neurons, respectively. The input consisted of three different angles: thermal gradient, crystal orientation, and Marangoni effect. Moreover, prediction results for the grain-boundary tilt angle were given as output by the output layer. It was implemented on PyTorch, an open-source machine learning platform. The model's accuracy, i.e., training and testing performance, was calculated using mean squared error metric (MSE). The model was tested 20 times by randomly changing training and test sets to calculate the mean MSE and the corresponding variance [70].

4.13. AI in 3D Printing Metals. Few studies in past years showed how 3D metal printing is not consistent, repeatable, or traceable because of many independent variables. To solve those problems, AI can be adopted. In addition to solving the problems mentioned above, it will also help improve the technology. Due to AI, the printers learn with the help of fed data to make assumptions and take decisions like assembling correct parameters independently. To observe the internal process and control it, sensors and cameras are accommodated at the nozzle in the printer. The observed data are fed into specific software for measuring and analyzing the multiple real-time builds. This method helps the printer learn and understand the problem and therefore find the best solution using AI. When the machine can understand the relation of one parameter to another, it can decide which parameter will be best to get which output [71].

4.14. Decision Support Systems in Laser-Based Additive Manufacturing. The modern technology of laser-based metal products AM using powder compositions comprises theoretical models and a lot of experimental data. A decision support system (DSS) can be used for the laser-based AM process [72].

The input comprises the type of process, the equipment for the process, and terms of reference while operating, such as the shapes, structures, characteristics of the product, the characteristics of the processed part, its geometric form, and the chemical composition properties. The output information includes settings of the controlled process parameters, the laser power, the laser emission mode, beam diameter, linear velocity of the laser beam on the metal surface, offsets between the layers, powder flow rate, carrier, shielding, compression gas flow rate, and characteristics of the substrate. The corresponding ontologies inspire the database and the knowledge base. The database contains information about the components of the AM system and the materials required for AM. The software components include editors for the creation and maintenance of the DSS, the tools for structuring the cases, the control parameters of the process, and the interaction between the DSS and the external tools of the mathematical modeling of physio-chemical [72].

5. Results and Discussion

5.1. DED Process and Advancements. While directed energy deposition is gaining popularity, many researchers are quite enthusiastic about conducting various types of research on this topic. The most desirable intention is to improve the process in whichever way possible by analyzing different outcomes of different research studies until we reach certain favorable process parameters. One such research was conducted by Heigel et al. to develop a thermo-mechanical model of the DED process with Ti-6Al-4V as the feed material. Many researchers consider free convection on all surfaces while creating a thermo-mechanical model. That may not result in accurate simulation results. Here, the measurement-based convection model is done with three depositions with different geometries and dwell times. An additional model is developed using the assumption of free convection on all surfaces. The difference in the results shows why a measurement-based convection model is required to produce accurate simulation results. An Optomec LENS MR-7 system is used with 500 W IPG Photonics fiber laser for the three depositions [73]. An argon atmosphere is created with an argon jet of 30 L/min capacity with an oxygen percentage less than 15 parts per million. The Ti-6Al-4V powder (44–149 μm diameter) is supplied by four jets with a combined flow rate of 4 L/min. After all the three depositions, the forced convection model produced more accurate results with an error rate of 10.4%, whereas the free convection model had an error rate of 43.8%. This shows that the measurement-based forced convection model generates more reliable results than the free convection model. Even though the measurement based on forced convection is efficient, it can be improved in some ways the authors prescribe. The mechanical model can be improved by performing more detailed measurements to explore the effects of specific part geometries on convection. Also, we can use approved CFD analysis to validate the CFD of the gas flow. This work also indicates that a more detailed mechanical model is required as this model produces accurate deflection in only one of the cases, despite having superior thermal results. Similarly, Yang et al. developed a three-dimensional Ti-6A-4V elastic model to check the thermo-mechanical behavior in the laser energy net shape (LENS) process. The quasi-static and dynamic analysis has been predicted using the FMEA process. The comparison of experimental and simulation of quasi-static and dynamic analysis is performed. They both compared mechanically to reduce computational costs. Mesh analysis is performed, and it consists of 6094 elements and 10378 nodes. The laser used in this process is 400 w IPG fiber laser, and its intensity is around 300 W [74]. Determining the thermal characteristics of the melt pool and solidification parameters is also important to get a consistent and fine microstructure. However, determining them using the current methods is a lengthy process and takes up much time. Huang et al. researched rapid prediction of real-time thermal characteristics, solidification parameters, and microstructures in laser DED. This research correlates localized transient thermal characteristics such as cooling rate, temperature, and so on and solidification parameters like thermal gradient and solidification rate to the process parameters for rapid prediction of the microstructural evolution. This correlation is validated by depositing stainless steel 316 L and Inconel

625 and conducting experiments on them. This research is conducted by using LPF_AM apparatus with Inconel particle size of 45–125 μm. 1.1 kW IPG Photonics fiber laser is used for creating the melt pool. The measured temperatures of the melt pool were well in coordination with results obtained from various previous research studies at various speeds and different energy densities. It was found that the DAS (dendritic arm spacing) is more delicate to scanning speed than the laser power. Also, this research found that high scanning speed and lower laser power result in a finer microstructure. Better microstructures were found in the top zones for SS 316 L and Inconel 625 due to cooling rates from the bottom to the top. The count time for the cooling rate ($G \times R$) and G/R proportion is found to be around 40 ms with a tolerance of 10-3 in this experiment, affirming the capability of this work to be utilized for the in situ forecast of warm and hardening qualities [75]. Xu et al. studied that AM process slicing method is used to improve quality and eliminate support structures. There are three types of slicing methods: powder, multi-directional, and non-layer-wise slicing methods. Few traditional processes are efficient to prefer in the powder bed fusion (PBF) system because they require costly support in the DED process. The multi-directional and non-layer-wise methods are used to achieve quality and require costly support. In the traditional slicing method, the contour extrapolation method is used to slice solid models, and the step-wise uniform method is used to slice CAD models to achieve high surface accuracy. To build desirable shapes with shorter build time, the accurate exterior and fist interior method is used. Local adaptive slicing is used to reduce fabrication time and maintain high surface quality. To build normal complex parts, decomposition-regrouping slicing time has been used, but their method is inefficient for making inner holes. The multi-directional slicing method is used to build parts without support structures and increase the quality of the surface. A non-layer-wise method is used to build components without support structures (Table 7). So, it saves material costs [76].

In situ monitoring is used to understand the physical phenomena. It influences process parameters such as porosity formation and powder flow. High-velocity X-beam that uncovers the laser-matter collaborations in different methods of DED preparing can help in the approval of warm, thermo-liquid dynamic, and thermo-mechanical models. A piezo-driven powder delivery system that controls power delivery in the AM process influences the geometry of the melt pool and mechanical behavior. High-voltage amplifier controls piezo element and vibration which induces gravitational flow. A surface strain of the softened pool entrains particles on the surface to enter the pool or discharges hot particles. Particles that stream into the dissolved pool impact the strength of the laser-instigated hole and the encompassing melt pool. Changes in mass entering the softened pool impact the cooling speed of the softened pool, reaching up to 106 k/s [77]. Hsu et al. worked on a publication that proposed a trinocular vision-based review framework to assess the cladding stature in the DED interaction utilizing a reference point estimation technique. The exactness of the proposed technique has been improved by using an alignment bar procedure to redress for the FOV impact and viewpoint marvel. Strikingly, the proposed technique is vigorous toward test arrangement mistakes and is computationally direct and exact.

Notwithstanding, the technique depends on the utilization of picture finders with the worthy goal since, something else, the unit distance addressed by every pixel in the caught picture is extraordinary in various districts of the picture. Consequently, the straight suspicions fundamental to the proposed estimation calculation presently do not hold. In executing the proposed estimation strategy, a separating strategy is utilized to eliminate commotion and the undesirable foundation locales of the caught pictures. Using infrared cameras to catch the soften pool picture may give more exact estimations of the cladding stature than those acquired utilizing the computerized cameras utilized in the current examination since the noticeable range comprises many noises. Be that as it may, an infrared camera is significantly more costly than an advanced camera.

Moreover, the outcomes acquired utilizing the present computerized cameras go amiss by close to 4.2% from the specific outcomes acquired utilizing an optical 3D scanner and caliper [78]. Hence, this outcomes the technique proposed in this examination gives a minimal effort which is helpful and the exact methodology for estimating the "cladding tallness" in the DED process. Laser beam additive manufacturing (LBAM) processes can be employed to generate practical parts via layer-wise-cladding to provide a chance to generate complex shaped parts and functionally graded parts that are utilized to build a variety of engineering components. Thompson et al. focused on thermal phenomena during the fed direct laser deposition (DLD) process. In AM metallic parts, PBF and DED processes are the most feasible methods. In PBF laser, selective laser melting (SLM) is used to create metallic parts. PBF is used to finish parts with more refined quality. The DLD process is used to produce parts, but it requires post-processing to get high surface quality parts. Not only surface quality, but this process is advantageous to get overhanging parts. In the PBF process, the powder acts as support, which does not require any other supporting structures. Both single and multi-nozzle can be used to feed powder [79].

Types of lasers used are neodymium-doped yttrium aluminum garnet (Nd: YG) laser and C02-type end pulsed-wave lasers, as shown in Figure 17. Nd: YG laser power ranges from 1 to 5 kW, and CO2 laser has capacities near 18 kw. There are two types of feed materials: powder and wire. Mainly DLD process has been commonly used to get finer deposition. Both DLD and PBF-L processes are operating in the inert gas chamber. This process utilizes an electron beam in a vacuum chamber. Challenges in the DED process are DLD efficiency, DLD control, numerical modeling, process parameters, industrial adoption, process monitoring limitations, DLD graded materials, and near net shapes. NNS is perfectly manufactured in the DLD process, and no further machining process is required. Both PBF-L and DLD are appealing added substance-producing strategies for metals since their working chambers should be cleansed with inert gas. Powder-bed and DED methods that

TABLE 7: Types of slicing methods (advantages and disadvantages).

| Category	Feature	Advantage	Disadvantage	Ref.
Adaptive slicing	Constant layer height.	(i) Easy application. (ii) Highly versatile.	(i) It can handle only simple geometric parts. (ii) Rough accuracy.	[76]
Basic slicing	(i) Accuracy or complexity requirement. (ii) Different layer heights concerning surface.	(i) High surface quality. (ii) Easily applicable.	(i) It cannot handle overhangs. (ii) Complex structures are still restricted.	[76]
Non-layer-wise slicing	(i) It requires fewer support structures. (ii) Multiple depositions.	(i) Reduces support structures. (ii) Complexity in several directions.	(i) It may need a manual inspection.	[76]
Multi-direction slicing	It does not require any support structures.	(i) No need for support structures. (ii) Implement Complexity in infinite direction.	(i) Lack of universality.	[76]
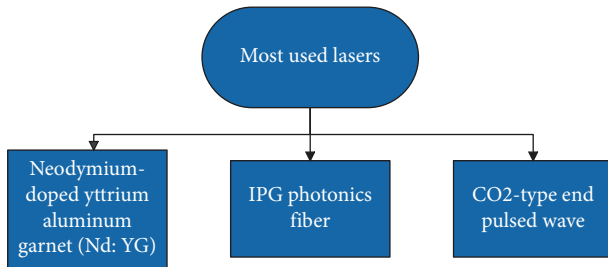
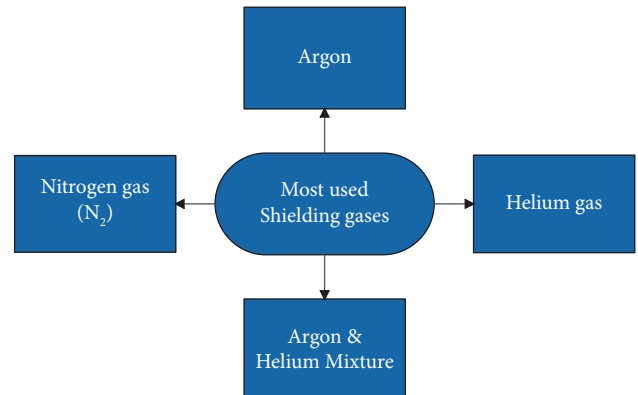FIGURE 17: Frequently used lasers.

FIGURE 18: Frequently used shielding gases.

use electron radiates require chambers with full vacuum conditions, which are regularly more exorbitant [79].

A lot of research was done on materials like Ti-6Al-4V, stainless steels, and Inconel, and aluminum and its alloys are the most used materials. One such research was done on Al-Si alloys by Javidani et al. Al-Si alloys are most suitable for welding purposes and hence are one of the most used materials in many applications. In this research, AlSi10Mg powder particles were deposited layer by layer on the substrate using 500 W IREPA IPG Photonics fiber laser along with a powder hopper as the material feeder. 45–90 μm was set to be the acceptable range of particle size for the deposition. According to the authors, the final deposition was nearly defect-free. It was found that cellular dendrites were found in the region near to the substrate, followed by columnar dendrites in the middle layers and then equiaxed dendritic morphology in the topmost layers of the deposit. The hardness test results showed that the region nearer to the substrate (cellular dendrites) showed the highest hardness value (nearly 65 HV) and the topmost layers (equiaxed dendrites) had the lowest hardness value (nearly 53 HV) due to its coarser microstructure [80]. It was also found that the microstructure was coarser near the boundary layers than the layers closer to the core. This work has proved that the DED process can efficiently print Al-Si alloys for many applications. The DED process finds many applications in fabricating thin-walled honeycomb structures and complex heat exchangers having thin walls. These applications are accomplished only when the walls created are fragile. One such work conducted by Jinoop et al. focuses on DED's

ability to fabricate thin walls using the LAM-DED process and Inconel 718 as the feed material. A 2 kW in-house developed fiber laser is used in the LAM-DED system. The substrate is sandblasted SS304L (10 mm thick, 75 mm diameter), which is fixed on a 5-axis CNC laser workstation. Argon of 99.99% purity is used as the shielding gas with oxygen less than 2 ppm, nitrogen less than 3 ppm, and hydrocarbons less than 0.2 ppm. The flow rate of the shielding gas was set to be 6–8 L per min for all the experiments (Figure 18).

Widely available IN718 powder with particle sizes ranging from 45–106 μm is used. After the final part is created, it is soaked for 1 hour at 950°C and then water quenched. A similar post-treatment is done to another final component where it is soaked for an hour at 1050°C and water quenched. It was found that the maximum laser energy per unit length (E_{max}) is 210 kJ/m, and the minimum of the same (E_{min}) is around 105 kJ/m. Also, the maximum powder feed rate per unit length (F_{max}) is 12.5 g/m, and the minimum value for the same (F_{min}) is around 4 g/m to fabricate defect-free thin walls. The walls had a dendritic microstructure free from any defects. The ideal process parameters for uniform deposition and high deposition rates were 1400 W laser power, a scan speed of 0.01 m/s, and a 0.117 g/s powder feed rate. Post-heat treatment processes resulted in reduced residual stress on the surface of the

component. While the as-built component had residual stress of 512 ± 15.46 MPa, it was reduced to 422 ± 12.99 MPa when heat-treated at $950°C$ (HT950) and was further reduced to 254 ± 11.80 MPa when treated at $1050°C$ (HT1050). This means that the residual stresses are reduced by 50% after the heat treatment process. Due to post-heat treatment, the surface microstructure was found to be recrystallized. The ductility increased by 62.5%, while the hardness is reduced by 12% [81]. Also, the energy storage capacity is increased by 2.4 times. This proves that the LAM-DED process is suitable for the desired applications and can be effectively used for thin-wall fabrication.

Saboori et al. studied microstructures and mechanical performance of DED AISI316L stainless steel. DED has an advantage in fabricating near net shape and high functional components. DED provides high valued parts for different engineering applications. However, there is a lack of knowledge regarding the mechanical characteristics and microstructure of built parts. There are different deposition patterns due to motion between deposition head and substrate. Because of its high deposition rate, this process is widely used to build large components. Demerits of the DED process show low powder efficiency, and roughness of surface should be done by machining process. The thermal history of DED, such as temperature gradient, high cooling rate, and high heating rate, defines the size of grains in DED components. Since all these parameters are important to build parts, effective parameters such as temperature gradient and local solidification rate at solid/liquid interface define the microstructure's solidification. The cooling rate at 103 to 104 k/s can get desired microstructures and mechanical properties in DED components. During heat transfer in the DED process, it is found that columnar structures grow in the direction of a thermal gradient, which dominates the middle height of the sample. Higher microhardness and finer microstructure are formed at the bottom top of DED components. There is a possibility of affecting thermal history due to the cooling rate, and it is one critical process. The cooling rate in DED of AISI316L ranges from 103–104 ks, which has a typical cooling rate. When the laser power increases, the average primary cellular arm spacing (PACS) of AISI316 produced in DED ranges from 3 to 9 μm. In order to reduce oxidation content, these should be done in a reliable atmosphere. From an industrial point of view, mechanical properties such as hardness and tensile properties are the main quality indicators. The main factors in achieving high mechanical properties are to reduce grain size and dendrite size. The building parameters such as feeding rate, scan feed, and laser power are key factors to improve quality. The factors that affect tensile properties are texture, elongated dendrites, and grain morphology. The powder quality influences porosity and consolidation and plays an important role quality of the component. The high mechanical properties can be gained when this process is held in N2 filled chamber. However, inert gas can affect the microstructure of the alloy. The different heat treatment

process is carried out to reduce internal stress. AISI316L, with high corrosion resistance and good mechanical properties, is used in different sectors, such as the petrochemical and automotive industries [82]. The DED process can fabricate customized and complex parts and prototype metallic parts and repair valuable components that traditional techniques cannot repair. Titanium is a commonly used alloy in aircraft, aerospace, biomedical, and automotive industries because of its corrosion resistance, significant strength, and fracture toughness. However, it is challenging for some applications due to its low thermal conductivity, which results in poor machinability. The ratio of thermal gradient (G) and temperature gradient (R) affects the shape of solidification, whereas thermal gradient and temperature gradient affect microstructure dimensions. The low ratio of G/R shows the equiaxed morphology of grains, and the high ratio of G/R shows the predominant morphology of grains. The G and R values are affected by several factors such as material features, machine condition, and other process parameters [83]. Ti-6Al-4V structures produced by the DED process are porosity-free components using high laser power and low powder-free rate. Thermal gradient and cooling rate influence the microstructures of Ti-6Al-4V components. It is important to know the thermal history of components because it affects the anisotropy of microstructures. Stainless steel is one of the major feed materials used in DED processes. DED fabricates many stainless-steel parts that are widely used in many real-world applications. Therefore, there is a high risk of the material being corroded in the long run. Hence, the corrosion properties of the stainless steel made through DED processes need to be studied to come up with solutions to reduce it in the future. One such research was conducted by Melia et al. on the corrosion properties of SS304L and compared with wrought SS304L to assess its effectiveness against corrosion. Commercially available SS304L powder with a diameter range of 45–90 μm is used as the feed material. Two types of DED systems are used in this research. One is a low-power (LP) DED using an Optomec LENS MR-7, and the other is a high power (HP) DED using a home-built high power and deposition DED system. Heat input given to the LP system is 0.03 kJ/mm, whereas the heat input for the HP system is decided to be 0.45 kJ/mm. The resulting parts were tested for corrosion using techniques like potentio-static holds, cyclic potentiodynamic polarization, and double loop electrochemical potentio-kinetic reactivation (DLEPR). The SS304L that is finally deposited showed microstructures having scattered nanoscale oxide particles, lack of fusion (LOF), and gas porosity. It was found that the LOF pores created can act as crevice sites and affect the part's corrosion resistance. The intra-dendritic parts control the breakdown resistance. In the absence of LOF pores, the Eb of the HP process was 100 mV lower than that of the LP process. The SS304L part produced by DED showed lower corrosion resistance than wrought SS304L due to LOF pore formation in the microstructure. The authors suggest that corrosion resistance can be enhanced considerably by minimizing LOF defects and achieving higher

cooling rates. The authors also suggest long-term research in this area for those materials to be useful in corrosive environments [84].

5.2. Process Parameters: A Guide to Efficient DED Process. Using the currently available literature, the process parameters are designed to lead to an efficient DED process. These parameters guide the researchers to understand the process and execute it efficiently concerning the core mechanical process.

(1) Many researchers have used a home-based DED system that uses different parts from various companies connected as a single system. This is a much better way to reduce costs than to use 3D printers from certified companies like Optomec. While this method effectively reduces costs, it has many notable drawbacks that can affect the research results. This is because of the following reasons. The first and foremost reason is that home-based DED systems are not reliable. Using cheap parts can result in fluctuating laser power and scan speeds. High laser power and scan speeds mean coarser microstructure and larger DAS (dendritic arm spacing) [75]. Using home-based DED systems can also lead to varying powder feed rates, resulting in irregular depositions and overlapping layers. Even though costly, using reliable DED systems such as Optomec LENS MR-7 is much better due to their stability in the long run. These 3D printers use a CNC control system (3 axes or five-axis) to better position the deposit on the substrate. It uses inbuilt 500 W IPG Photonics fiber laser which constantly delivers laser with a power of 410 W. This laser is also upgradeable to 1 kW if needed. These premium printers are also equipped with thermal imaging cameras with analysis software. This feature is beneficial to determine the number of thermal stresses on the surface of the part. These systems come with a better atmosphere control to monitor shielding gas and oxygen in the gas chamber. Home-based DED systems cannot monitor the amount of oxygen in the inert gas chamber with such accuracy, and the melt pool may oxidize if the amount of oxygen is high. Systems like Optomec LENS MR-7 also come with more powder feeders to create parts with different materials. Every layer can be different from the previous layer. Therefore, the use of a proper DED system is essential to ensure correct results and successful research.

(2) Heat treatment shows different characteristics of tool steel in the DED process. However, the heat treatment process is used to improve the mechanical properties of components. Tool steel such as H13 and D2 was deposited on the substrate using the DED process as the hardness of deposited H13 steel is higher than a wrought H13 steel substrate. At the same time, the hardness of deposited D2 is lower compared to wrought D2. Microstructures and heat treatment vary with different materials used in DED. For Ni-based alloys, post-weld heat treatment is carried out to relieve stress from materials and increase strength. For steel, heat treatment is carried out to get relief from residual stress and grain refining. The mechanical properties such as hardness, tensile strength, and impact strength can be improved using heat treatment. As research studies suggest, heat treatment can eliminate boundaries between newly deposited layer and pre-existing layer. It seems that after the heat treatment process, microstructures of H13 steel were changed and similar to wrought H13 steel. Both microstructures seem to be tempered. Martensite and XRD results show that the phase of H13 steel was ferrite. After heat treatment, the equilibrium of H13 steel was austenite and maintains the temperature at 1293 K. After heat treatment, the chemical composition of deposited H13 and wrought H13 seems to be similar. However, the microstructure of D2 steel is dendritic and eutectic. The microstructure of deposited D2 and wrought D2 is different. The deposited D2 consists of fine carbide, which is dissimilar to wrought D2. However, wrought D2 has martensitic structures. The microstructures without heat treatment process consist of columnar crystals [85]. During the printing process, materials can gather tension and internal stress, which affects mechanical properties. Such effects can be reduced by heat treatment. So, it can provide external features such as tensile strength and heat resistance. The value-based heat treatment process can benefit alloys such as titanium alloys, stainless steel, nickel superalloys, and so on [86].

(3) Selection of the type of feed material is also very essential in DED processes. The feed material can be a wire or powder according to the type of outcome desired by the researcher. In some cases, using a wire or powder does not matter to the researcher as long as the material is being deposited on the substrate. In such cases, powder feeding can be used because powders of most metals and ceramics are widely available in the market. However, one major drawback of using powder-based feed materials is that the powder capture efficiency is always less than 100% [87]. That is, all the powder that is fed into the feeder is not captured in the melt pool. Therefore, the excess powder is utilized. Also, the thickness of the deposit made by powder feed is more than the thickness deposited by wire feed. This thickness helps overcome some wrinkled surface physiography associated with directed energy deposition. If the amount of feed material is one of the essential characteristics considered in detailed research, it is always advisable to use wire-based feed material because the wire capture efficiency is nearly 100%. When particular research involves fabricating basic geometries, either thick or thin, and some block-like structures, it is better to use wire feed. Wire-based

feeds produce pore-free parts so that the densities of the parts produced are high compared to parts made by powder feed. Wire-based feeds indeed produce parts with lower dimensional accuracy when compared with powder-based wire feeds. This can be significantly improved by controlling the process parameters such as wire feed rate and wire thickness. The optimal process parameters for doing this varies for different materials and can be found through further research. Therefore, if the surface texture and quality are not an issue, wire-based feeds are the best way to reduce material wastage and create parts with greater densities.

(4) Layer thickness is one of the most critical process parameters which build components layer by layer in the AM-DED process. Layer thickness can be determined based on the single-layer height given during deposition. Layer thickness plays a significant role in maintaining the strength and good surface quality of the component. The DED technology involves two kinds of energy sources: laser energy and electron beam, to build metallic components layer by layer. It can be used for part repair or to build new parts. As many researchers said, the geometry and structure of components depend on the thickness of the layer. An increase in melt pool volume and reduction in layer thickness can have benefits over roughness. The slicing strategy can help in the decrease in manufacturing time and depositing layer thickness depends on process parameters.

(5) Layer thickness improves not only the accuracy of geometry but also the mechanical properties of components. The main disadvantage of slicing in the DED process is that it requires additional machining processes to improve accuracy [88]. There are three slicing methods: feedback control, conventional, and adaptive slicing methods. The conventional method can reach target height till 1.5 mm and adaptive slicing can reach target height till 1.82 mm. In steel, micro-hardness increases from the first layer to the top deposition layer. The top layer shows the highest hardness. The layer height can increase either due to energy source or powder feed. Feedback control relents the performance concerning geometry. The conventional and adaptive method is also called an open-loop process. The open-loop process sets defined values, and there is no feedback from process output. Adaptive slicing is a beneficial method to build quality parts and decrease production time.

(6) One of the significant process parameters in the directed energy deposition process is laser power. The amount of laser power used in the system determines many essential attributes, such as the size of the melt pool, the density of the deposit, and its thickness. Firstly, increased laser power leads to increased melt pool size. This is because as the temperature of the melt pool increases, the material expands to a specific limit, increasing the melt pool's

size. An increase in the size of the melt pool means a reduction in density [89]. Therefore, when this melt pool is deposited, it covers more area on the substrate, and hence the height track width will increase. The laser power shows its effect not only on the melt pool but also on the substrate. Generally, the laser slightly melts the substrate to create a better bond with the deposit. This is known as dilution. If the laser power is high, the substrate dilution increases, and therefore the depth of penetration increases for the deposit. This results in lower deposit heights than planned by the researcher. Also, lower laser powers (100 W–400 W in general) lead to the melt pool's rapid solidification. Even partial solidification of the melt pool increases the density on the whole. Many researchers found that scale formation can be created on the deposit's surface due to the melt pool's rapid solidification [90]. Sometimes, deposits with smooth surfaces or low surface roughness are the required attributes for researches. In that case, it was found that high gas flow rate combined with high laser power can deposit materials with low surface roughness. Finally, it was found that crucial output parameters such as clad thickness, dilution, temperature, and thermal stresses will increase with the increase of the laser power. Of these parameters, dilution and temperature become constant because they reach a point called the saturation level [91].

(7) Powder flow rate is essential to improve reproductivity and reliability in industrial applications. Due to the lack of sensors, it became difficult to measure powder flow rate. However, these days, many different methods have been introduced to measure powder flow rate. Industries use the equipment called weight-loss metering system to regulate the powder flow rate. The online powder flow rate is not recommended because of the low powder flow rate. The optoelectronic sensor is used to sense powder flow rate, and it consists of a photodiode, glass window, and laser diode. The laser energy is used to regulate power flow, and it sends process feedback signals. Another sensor, such as a compact pressure sensor, can be used to sense powder flow rate, and this high flow rate requires high pressure. Suppose there is a constant powder flow rate deposited at a point that causes dilution and porosity. The variable powder flow rate (VPFR) is the best strategy to adopt because the idea of VPFR is the constant distribution of powder along the path. It even helps to measure uniform morphology if the system decelerates or accelerates. The powder flow rate system consists of a PC that controls the powder flow rate. The circle-shaped or fish-shaped parts were fabricated using three different powder flow rate references: variable-based, constant, and modified [92].

(8) Scan speed is yet another vital process parameter that can primarily affect the melt pool dimensions. There

is no ideal scan speed defined for a process. Optimum scan speed values change from one material to another material and one process to another process. However, lower scan speeds generally result in large melt pools with considerable build heights and meager dilution rates. When the scan speeds are low, the flexural strength improves remarkably due to reducing grain sizes and suppressing macroscopic cracks. High scan speeds have a decreasing effect on melt pool dimensions. An increase in scan speeds results in low melting or lack of fusion. So, a melt pool is not produced [93]. As scanning speed increases, clad height, temperature, stresses, and clad height decreases [91]. This is because there is low energy density or heat input due to less interaction time. At high scanning speeds, the thermal stresses decrease, and directional grain growth weakens, which causes significant suppression of the cracks on the part's surface. At higher scanning speeds, porosity increases due to an increase in molten pool viscosity. This increase in porosity notably decreases the strength of the final component. Also, with increasing scanning speeds, the fracture toughness of the final components increases. This is caused due to the microstructure refinement, and the flexural strength shows a parabolic course. However, using high or low scanning speeds can be neutralized using medium scanning speeds (400–500 mm/sec). By using medium scan speeds, the sample shows excellent comprehensive properties along with balanced toughness and strength.

5.3. Artificial Intelligence in DED. The results from the use of AI seem promising in the DED technology. AI has brought on a significant impact on the quality and efficiency of the technology while also reducing wastage. The results discussed from the experiments performed will help justify the impact of AI in this section.

The accuracies of the models were evaluated based on RMSE, RE, and the coefficient of determination (R^2). The LSTM prediction demonstrates the model's strength against noises. However, the XGBoost shows its relative weakness when there is variation or unsteadiness in the temperature. This resulted in line with spikes. The observed values for RMSE, RE, and R^2 of the model having XGBoost are 95.9, 3.7, and 54.4, respectively. Likewise, the three measurements of the prediction using LSTM are 88.2, 3.4, and 60.1. Compared to XGBoost, the RMSE, RE, and R^2 are improved by 8.0%, 8.1%, and 10.5%, respectively, on the model based on LSTM [56].

It was also observed that for temperatures below approximately 2000°C, the LSTM model generates more accurate predictions. However, for values above approximately 2000°C, both models (XGBoost and LSTM) fail to give highly accurate results [56].

From the seventh experiment, the laser power was 350 W with 11 mm/s of the scanning speed. The RMSE, RE, and R^2

TABLE 8: The difference in performance of LSTM and XGBoost.

Network/algorithm	RMSE	RE	R^2	Ref.
LSTM	88.2	3.4	60.1	[56]
XGBoost	95.9	3.7	54.4	[56]

prediction using XGBoost are 24.0, 1.0%, and 51.8%, respectively. Likewise, the RMSE, RE, and R^2 of LSTM are 20.1, 0.8%, and 67.1%. The prediction accuracy of LSTM over XGBoost according to the observed values of RMSE, RE, and R^2 is improved by a whopping 16.3%, 20.0%, and 29.5%, respectively. Given overall smaller variations, the model based on LSTM delivers much better performance than XGBoost [56].

Finally, it was observed that the model built with LSTM has higher accuracy than the model built using XGBoost. XGBoost is faster than LSTM, and so LSTM is suitable for smaller datasets. For the particular case in the experiment, LSTM was suitable, but this cannot be said for all cases [56]. From [3], we can have the following comparison as shown in Table 8.

The Levenberg–Marquardt algorithm, constructed using the TRAINLM function in MATLAB, was allocated 70% of the data for training, 15% for testing, and 15% for validation. It was found that the minimum MSE reached $10.6 \times 10-5$ (after four epochs), and the correlation coefficients for the areas; For training: 14 data is 0.983; validation: 3 data is 0.999; testing: 3 data is 0.999; overall data 20 runs are 0.987. As for mean absolute percentage error, the calculated value of MAPE for RSM and ANN is 0.587 and 0.188, respectively. Finally, it is determined that ANN performed significantly better than RSM, yielding better predictions. A decrease of 67.97% was observed in MAPE with ANN over RSM [94].

Two stacked RNN models were trained. The models were trained for 20 s and 50 s, and they were tested for 100 seconds of thermal history. The model trained for 20 seconds continues to make good predictions for about 60 seconds of thermal history, showing an MSE of $7.05e-5$ for the 100 seconds. The model trained for 50 seconds had only $3.17e-5$ MSE for 100 seconds of thermal history prediction. This decrease in MSE comes at the cost of more training time and resources [58].

The four tests show that an accuracy of 80% can easily be achieved in various tasks. This result shows that the model is effective in process monitoring. This also outperforms the DNN model in some situations. It is concluded that the DCNN structure is more suitable for problems related to thermal image processing in additive manufacturing [57].

The RNN model proposed by the authors is trained in different arrangements. This included the number of layers, GRU units, and fully connected layers. RNN layers: 1–5, GRU units: 100–500, and fully connected layers: 1–5. The model had an MSE of $1e-4$ after 100 epochs of training with a smaller number of layers. It reached an MSE of $3.210e-5$ on training and $3.84e-5$ on testing with many layers and units on 100 epochs of training. The time consumption for training was approximately 40 h on Nvidia Quadro P5000. Finally, the results showed that the

TABLE 9: A comparison of two training networks.

Network	MSE	Training time	Regression R-value	Maximum relative error (%)	Minimum relative error (%)	Mean relative error (%)	Ref.
BP-AM	$8.792E-05$	6 min	0.979	24.98	0.0018	7.745	[56]
LS-SVM	$2.89E-08$	0.016 s	1	0.7	0	0.18	[56]

model could reach $2.97e-5$ MSE on testing after 100 epochs of training [58].

In the width prediction, for sample 10, a maximum absolute error of 13.9 μm was found with a relative error of 8.2%. From FEM data, the average error of 6.88 μm was achieved for cracks of 50–170 μm. For sample 3, a max error of 18 μm was found. The prediction through artificial crack data was 7.41 μm for cracks of 56–160 μm. From FEM simulation and artificial crack data, it is observed that LSTM NN is pretty reliable. For this application, though, the combined technique of LSR-NN was tested to detect crack width of LENS with wear-resistant coating. The mean error of the prediction was 2.0 μm, and the max error was 6.1 μm for cracks of 3–68 μm [59].

LS-SVM, compared to BP-AM (Table 9), shows better ability in generalization and its strength in function approximation. Hence, LS-SVM is more useable in the LENS process for more accurate predictions [60].

With the help of the plots that compare the performances of CNN and BDT, BDT had a 68.73% background rejection, whereas CNN had 93.02% for 60% signal efficiency. This was for the 1st case. For the 2nd scenario, BDT had 86.84% background rejection against 96.39% CNN for 60% signal efficiency. CNN outperformed BDT for more considerable signal efficiencies [63].

Ever since the processing power proliferated, so did the field of deep learning. Numerous advanced techniques have taken a form and can outperform CNN as well. Caps Net is one of the examples which aims to make optimizations and enhancements to the CNN to handle the spatial relationship with more efficiency. Likewise, PointNet++ is another pioneering project that seeks to apply ML on point clouds (collection of high dimensional objects). Another such advancement is GNN which stands for graph neural network. This operates directly on graph functions and has found wide use in many physics-related applications, including high energy [63].

Using an ANN to model the correlation between microstructure and the Ti-6Al-4V alloy properties proved to be very efficient with absolute percentage errors between the predicted and experimental values less than or equal to 5.0%, which is an acceptable range. Moreover, the developed ANN model can predict the mechanical properties of Ti-6Al-4V alloy in the future [64].

Similarly, when compared the efficiency of GP, NN, SVM, and GBT models to predict single clad geometry, the Gaussian process (GP) model by the metrics was more successful, though only marginally, at regression and classification than neural network (NN) models. Support vector machines (SVMs) underperformed when compared against the GP model. SVMs, when compared to the

NNs, had lower variance and better classification accuracy. As a classifier, the GBT model outperformed the other models. As a regressor, GBT showed the lowest variance [66].

In another research, a CNN and an ANN successfully predicted tensile properties of Ti-6Al-4V, where CNN was used for feature extraction in thermal image data, and ANN approached to identify parameter effects. 84% of the data lay within the ±5% deviation from a perfect prediction of yield strength, 90% of the data lay within ±5.85% deviation, and 70% of the data lay within ±3.48% deviation. The median deviation was 2.4%, and the average deviation was 3.0%. The maximum error was calculated to be 8.2%. Most importantly, these data represented three distinctly different heat treatments which was never done before. The average knockdown effects due to texture for the alloy were calculated to be 3% using the wrought structure equation as a baseline [65].

For predicting surface characteristics in $CO2$ laser micro-milling of glass fiber reinforced plastic composite, ANN model with 3-6-6-3 network structure was the most efficient with the mean, maximum, and minimum prediction errors of 0.82%, 2.26%, and 0.0004%, respectively. The difference between experimental and model values of milling depth was within ±2%, and the coefficient of determination R^2 was found to be 0.999. For surface roughness, the difference between experimental and model values was again ±2%, whereas the value of R^2 was found to be 0.997 and 0.993 for parallel and perpendicular to the fiber during milling, respectively [69].

In another paper where an ANN model was developed to study grain-growth behavior, the MSE for the model was 3.45 and 6.42 for training and testing data, respectively. The average distance between the prediction of the grain-boundary angle and their experimental results was 1.83 and 2.43, and the standard deviation was 0.32 and 0.73, respectively, for training and testing. The tolerance range of this model was found to be about ±4. An average prediction error of 2.43 showed that a feedforward neural network is an appropriate tool for this task [70].

When incorporated with 3D printers, AI's resultant system helps aerospace manufacturers make more accurate and precise products like aero-parts, which are more flexible, less costly, and produce less waste [71].

In this ontology, the authors proposed a hybrid approach to solve the current problem of DSS in laser-based AM. The researchers combined the knowledge engineering methods and case-based search by analogy. This includes continuous updating of the knowledge base by experts for improvement in the process. This work was later implemented, and the

TABLE 10: Comparison between various network models used.

Algorithm used	Depth, layer sizes, training time, and testing time	Dataset	Accuracy	Variation from experimental value	Ref.
ANN	1 hidden layer, 7 neurons 3-7-1, feed-forward, backpropagation neural network model	Not mentioned.	98.7%	67.9% MAPE	[94]
CNN	(i) Avg pooling layer (ii) Convolution layer (3×3; 32 filters) (iii) Avg pooling layer (iv) Convolution layer (3×3; 16 filters) (v) Flattening layer (vi) Fully connected layer (vii) Softwax function (confidence values into probabilities)	The time-series thermal images were collected with the help of the cameras and other multiple DED process settings.	80%	Not mentioned	[57]
RNN	(i) 1–5 layers (ii) 100–500 GRU units (iii) 1–3 fully connected layers	Self-made using GAMMA.	MSE: $2.97e - 5$ after 100 epochs	Not mentioned	[58]
LSTM	(i) Input layer (ii) LSTM layer (iii) Fully connected layer (iv) Dropout layer (v) Fully connected layer (vi) Regression layer	FEM sim data and data from artificial crack experiments.	The average absolute error of prediction: $2.0 \, \mu$m	(i) Abs error for FEM data: $6.88 \, \mu$m (ii) Avg error for artificial crack data: $7.41 \, \mu$m.	[59]
ANN: feed-forward backpropagation	Input parameters: L0 orthogonal array Input variables: 3	Self-prepared, pre-processed, and labeled data	97.08% R-squared	Not mentioned	[60]
CNN	2 convolution layers: (i) Layer 1: 10 filters of kernel size 6×6; (ii) Layer 2: 20 filters of kernel size 4×4 max-pooled with pool size of 2×2 convolution ($20 \times 7 \times 7$) images $\longrightarrow$ max-pooling $\longrightarrow$ fully connected layer (with 200 nodes) $\longrightarrow$ activation function RELU $\longrightarrow$ 50% dropout	100,000 images of both classes. Training images: 60,000	96.02%: case one 93.69%: case two	24%: case one 9.6%: case two	[63]
Stacked RNN	(i) 1–5 hidden layers (ii) 100–500 GRU units (iii) 1–3 fully connected layers Training time: 40 h on Nvidia Quadro P5000	Built using GAMMA.	MSE: $3.17e - 5$	N/A	[58]
ANN	Single hidden layer (3-16-4)	Trained dataset using ANN backpropagation.	90%	5%	[64]
Neural network (I), gradient boosted decision tree (II), SVM (III), and Gaussian process (IV)	(I) For regression: linear neurons = 283, non-linear = 210, learning rate: 0.000871 For classification: linear neurons = 358, non-linear = 744, LR = 0.000465; 1 hidden layer. (IV) LR = 0.01; max depth = 20	Previously unpublished experimental results of this author. Input set (powder material, substrate material, spot size, power, Mass flow rate, travel velocity)	II > IV > III > I ensemble regression accuracy of 70.5% and an ensemble classification accuracy of 72.3%	Not mentioned	[66]

TABLE 10: Continued.

Algorithm used	Depth, layer sizes, training time, and testing time	Dataset	Accuracy	Variation from experimental value	Ref.
Hybrid of ANN and genetic algorithm approach	Not mentioned	Experimentally measured process variables.	84%	5%	[65]
ANN	Neural networks with hidden layer containing nodes in the following orders were tested: 3-1-3, 3-3-3, 3-6-3, 3-7-3, 3-1-1-3, 3-3-3-3, 3-6-6-3, 3-7-7-3	Prepared after conducting 60 experiments. Constraints like availability of material, cost, and time required for experiment were considered	82%	2%	[69]
ANN	1-5-10-1	50 groups of data were gathered from the experiment.	Not mentioned	4%	[70]

process of AM of metal products using laser-based tech was created on the IACPaaS cloud platform. This work has been used to date in various works, with the components of the knowledge portal improved further, helping to create new components and bringing improvement on the current ones [72].

Table 10 provides an exhaustive comparison between various network models used in the DED processes to date, and their accuracy, datasets, and various other parameters for industrial significance have been addressed and accumulated.

6. Summary and Conclusions

Based on the above results, we can conclude that AI has been beneficial in making various processes of DED easier. The products made using DED technology and monitored by the AI-trained system have become of superior quality. The products are superior, and also there are fewer failure rates as well as fewer wastes. With the suitable model and proper amount of training dataset, a system with accurate and reliable prediction can be prepared, which helps to make a good DED manufacturing technology. Throughout this literature review, we have seen high use of CNNs, ANNs, and RNNs based on the type of use. These network models have shown significant improvement in results compared to the results from the DED technology without AI. RNN architecture excels at predicting thermal history in the DED process. The CNN architecture excels at applications such as speech recognition, image processing, fault diagnosis, and feature extraction from high-dimensional signals. In DED, CNN can be used as a tool for pattern recognition and ultimately in process monitoring. The ANN architecture on the other hand is also a non-linear machine learning model that can effectively predict track dilution values in the DED process with different setting parameters. In our reviews, CNN showed accuracy in prediction as high as 96% and as low as 80%, while ANN also showed great fit with the R_2 value of 97%. The RNN is highly effective in predicting values in which the previous output affects the current output and has shown MSE as low as $2.97e-5$. Few algorithms like ANN are more useful when developing a

predicting model, but few others, like GBT, are more efficient when we need geometry prediction. GBT (gradient boost decision tree) is a technique in ML that effectively solves regression and classification problems which have data in tabular form. A prediction model is produced from a group of weaker prediction models where each model is optimized using a loss function, called gradient descent. NN and GBT have this optimization thing in common. Similarly, SVM and Gaussian process have a commonality too, as they both can be called kernel methods. In these processes, a kernel is produced among all the data, which can best describe all other data. SVM and GP can be disadvantageous as they do not provide probability estimates directly. Various parameters, like MSE, accuracy, variation, and standard deviation, make a basis for comparing the efficiency of all these algorithms. We have tried to present most of the efficiency determining parameters of the AI techniques used in the DED process. If studied further, we can explore many more techniques that are more efficient than those explained previously. These AI techniques can be used to achieve similar goals in areas other than DED. We can study more about AI and its contributions to mechanical engineering and improve already known techniques, as there is always room for improvement.

The directed energy deposition (DED) process and its key parameters are thoroughly discussed by reviewing various research or journal papers published in recent times. Firstly, the basic structure of any DED system is depicted as a well-labeled diagram showing all its components. As already discussed, there are two types of feed material in the DED process, namely, powder-based and wire-based, which are thoroughly discussed in the later sections. Also, there are three types of heat sources, namely, electron beam, laser beam, and plasma or arc. A brief description of the overall process is given as a flowchart which helps the reader better understand the overview of the process. The types of environments in which the DED system is conducted are also discussed as a flowchart showing all types of shielding gases or vacuum that create the environment. According to the flowchart, there are two shielding mediums—local shielding and inert gas chamber. Pros and cons of these shielding mediums are listed in a table. A vacuum chamber, even

though heavy and expensive, creates the best environment for the process. In mediums created by inert gases, an inert gas chamber gives the best results as it provides a better environment when compared to local shielding. Next, the DED process is compared with similar additive manufacturing processes based on their basic description, related technologies, and materials. Then, the major pros and cons of using the DED process are elaborately discussed. One of the main advantages of using this process is that it can be used for varied materials such as metals, polymers, and ceramics, and one major disadvantage is that the products made by this process have a relatively poorer surface finish than other additive manufacturing methods. There are three types of applications of the DED process in any industry. DED is used for the addition of features in pre-existing parts. It increases the value of the product and reduces machining times. This process is used in the repair of pre-existing components in many industries. In component repair, it reduces lead time and extends the life of the part. Also, the DED process is used to fabricate near net shapes where the material wastage is reduced while fabricating complex shapes.

Next, the types of energy sources—an electron beam (EBAM), a laser beam (LDED), and arc (ADED)—are thoroughly discussed. The EBAM process is done at a power range of 4–20 kW in a vacuum chamber. This process is mainly used to produce near net shape parts and large parts. While EBAM is used to produce large parts, the LDED process produces smaller parts with higher resolution. The powder is the primary feed material used in the LDED process. Many types of feed materials that can be used in the DED process were discussed one by one. The types discussed are pure metals, metal alloys, polymers, and ceramics. In pure metals, copper and tungsten are the two most used metals due to the following properties. Copper is majorly used as feed material in the LDED process. While copper is used in aviation and marine industries, tungsten is used in aerospace, space, and nuclear industries, such as wood and metal cutting, drilling, and machining, due to its excellent corrosion resistance, low vapor pressure, high thermal conductivity, high melting point, and higher density. Tungsten finds its uses as feed material in AM processes like powder bed fusion, plasma laser sintering, and LDED. The most used materials as the feed in any DED process are metal alloys. Some of the key metal alloys on which much research has been done are discussed in detail in this paper. Hastelloy-X is a nickel-chromium iron-molybdenum alloy that shows high mechanical strength, high yield strength, high ductility, and high corrosion resistance. Therefore, it is used to fabricate gas turbine engines, heat exchangers, etc. Moreover, it is used as feed material in the LAM-DED process. Inconel 718 is a nickel-based superalloy used to create jet engines, gas turbines, etc., as it has high tensile and impact strength and good resistance to corrosion and oxidation. It is mostly used as feed material in the LAM-DED process. Titanium-molybdenum (Ti-15Mo) shows excellent corrosion resistance, high hardness, and fatigue. Hence, this material is used as bioimplants and in aerospace industries. The EBAM-DED process uses this material as feed. Similarly, other titanium

alloys are also used in similar military, aircraft, and aerospace industries due to their high tensile strength and toughness.

Stainless steel is one of the highest standard alloys that is used almost everywhere. It has high resistance toward corrosion and displays high strength even at high temperatures. It is mainly used as feed material in the EBAM-DED process. Zirconium alloys such as Zircaloy are used to create parts in the nuclear industry, water reactors, etc., due to their high ductility, hardness, and corrosion resistance. Also, some aluminum alloys, such as 4043 aluminum alloy, display good corrosion resistance and are used in welding and brazing metals. The DED process is not only applicable to metals and metal alloys but also polymers and ceramics. Some of the most used polymers in the DED processes are discussed in detail. One such material is polymethyl methacrylate (PMMA). It is shatterproof, rigid, UV and harsh weather-resistant, and highly resistant to scratches. These properties are used in the biomedical industry, automotive and transportation industries, and the furniture industry.

Selective laser sintering (SLS) and DED processes use this material as a feed material. Polyether ether ketone (PEEK) is a polymer with high heat and electrical resistance to withstand high temperatures. Therefore, it is used in the medical industry, aircraft, and automotive industries. Even though it can be used as feed material in the DED process, it is mainly utilized in the fused deposition method (FDM) process. Another important polymer is acrylonitrile butadiene styrene (ABS). It is used in the automotive industry, pipes and fittings, and structural applications due to its high impact strength and heat resistance, high strain resistance, and stability over time. Polypropylene (PP) has excellent barrier properties, low cost, low moisture-vapor transmission, exceptional optical clarity, and high bacterial and thermal resistance and is used in the packaging industry, automotive industry, and medical industry. SLS process uses this material as feed to fabricate components in these industries.

Moreover, finally, polylactic acid (PLA) is a biobased, biodegradable, biocompatible, compostable, and non-toxic polymer used in the packaging industry, health and medical industry, and many structural applications. Some of the ceramics are also used as feed materials in the DED process. One such ceramic is alumina which has high electrical insulation and resistance to corrosion. Hence, it is used in automotive sensors, dental implants, and electronics. It is mainly used as feed material in the LAM-DED process. Another ceramic that is widely used in the DED process is zirconia. It has high toughness, high strength, and corrosion resistance and is used in producing dental crowns, insulators, rollers, pistons, etc. Another ceramic widely used in the DED process is magnesium aluminate spinel which is used in bulletproof glass, aerospace, and defense industries. It is mainly used as feed material in the LAM-DED process.

Then, a wide variety of works done by many researchers are thoroughly studied, and their research outcomes are drafted in this paper. While many researchers discussed the thermal effects of laser power and scanning speeds on the

weld pool, some focused on a trinocular vision-based system that can measure the clad height in the DED process. One of the main results presented in these papers is that a measurement-based forced convection model can produce meager error rates. This model can be used for any research work that focuses on thermal characteristics. A CFD analysis can also be added, and high scanning speed and lower laser power are always preferable to achieve finer microstructures while working with stainless steel and Inconel. It is established that a trinocular vision system is always better than a binocular vision system which gives a minimal effort and helpful and exact methodology for estimating the cladding tallness in the DED interaction. Also, many papers tried to find out the types of materials that can be used as feed in the DED process. Many researchers tried and are still trying to fabricate defect-free components of various metals and metal alloys through the DED process. Metal alloys such as AlSi10Mg are proved to be very suitable as feed materials in the LAM-DED process as they showed higher hardness values than the AlSi10Mg parts created by other manufacturing methods. Many studies were inclined toward finding the properties of final parts created by the DED process. This includes finding out the final hardness values and corrosive properties in which it was found that stainless steel that are fabricated from DED processes. They have less corrosion resistance than parts manufactured through traditional methods and their thermo-mechanical properties and other various other properties may vary. It is also seen that slicing is a critical but less used process in additive manufacturing processes such as DED.

Slicing can be very useful to increase the quality and eliminate support structures. The types of slicing processes, namely, additive slicing, essential slicing, non-layer-wise slicing, and multi-direction slicing, are exhaustively discussed with the help of a table and concerning their features, advantages, and disadvantages. Also, three types of laser beams are extensively used in DED processes. IPG Photonics lasers, neodymium-doped yttrium aluminum garnet (Nd: YG) laser, and C02-type end pulsed-wave laser were used. These are depicted as a flowchart in the part of the discussion. There are four mainly used shielding gases in the DED processes. They are argon, helium, argon-helium mixtures, and nitrogen. These, too, are depicted as a flowchart in the part of the discussion. Finally, to improve the quality of the components, the building parameters such as feeding rate, scan feed, and laser power are vital factors [41, 95–98].

After studying and analyzing many research works, a set of process parameters that can be useful for a particular process is drafted and discussed in detail in the process parameters section. The first and foremost process parameter discussed is that using certified or reliable DED systems is always better than cheap or home-based DED systems. This is because cheap DED systems can have a fluctuating laser power or powder delivery rate, whereas reliable DED systems can provide constant rates at all times. Also, relevant examples are given from research papers to justify the same.

The second process parameter tells that post-heat treatment processes are essential to enhance the mechanical properties of materials such as hardness, tensile strength, and impact strength. Adverse effects such as tension and internal stresses can also be removed using post-heat treatment processes. This is proven for two types of tool steels – H13 and D2 in the recent research works conducted, which is also mentioned in the process parameters section [99–104].

The third parameter is about the selection of feed material in DED processes. There are two types of feed material—wire and powder. The advantages and disadvantages of both wire and powder feed are discussed in detail, and it is seen that powder-based feed is best suitable for the LDED process, and wire-based feed is used when the material wastage is not to be encouraged. The difference between them is also discussed in length. The following process parameter is about the layer thickness of the deposited layer in the DED process. It is said that the geometry and structure of components depend on the thickness of layers. Lower thickness and increased melt pool volume produce components with better roughness. The fifth process parameter is about the laser power and how it affects the geometry of the component. Higher laser powers (800 W+) mean increased dilution and penetration depth, which reduces the total component's height. At the same time, lower power (100–400 W) leads to rapid solidification of the melt pool, increasing the deposit density. Scale formations can be seen in such deposits. Finally, it was found that crucial output parameters such as clad thickness, dilution, temperature, and thermal stresses will increase with the increase of the laser power. Of these parameters, dilution and temperature become constant because they reach a point called the saturation level. The following process parameter is about the powder flow rate of DED processes. Monitoring the powder flow rate is essential to improve the reliability of components in industries. Many different types of methods are mentioned which can efficiently measure the powder flow rate. Maintaining constant flow rates at all times is very important to regulate dilution and porosity. Even distribution of powder feed is also essential [19–23, 105–107].

The final parameter discussed in this review talks about the scan speeds of lasers in the DED process. Lower scan speeds result in significantly large melt pools with considerable build heights and meager dilution rates, whereas increase in scan speeds results in low melting or lack of fusion [108–113]. So, a melt pool is not produced. As scanning speed increases, clad height, temperature, stress, and clad height decrease. However, using high or low scanning speeds can be neutralized using medium scanning speeds (400–500 mm/sec). By using medium scan speeds, the sample shows excellent comprehensive properties along with balanced toughness and strength. Also, the role of artificial intelligence (AI) is an added flavor to the directed energy deposition process and has a scope that is very promising shortly. Recent signs of progress in artificial intelligence have made it a technology that can be used in any

application with the DED process as no exception to reduce the human effort [114–116].

Data Availability

The data used to support the findings of this study are included within the article.

Conflicts of Interest

The authors declare that they have no conflicts of interest.

References

[1] G. Kou, H. Xiao, M. Cao, and L. H. Lee, "Optimal computing budget allocation for the vector evaluated genetic algorithm in multi-objective simulation optimization," *Automatica*, vol. 129, Article ID 109599, 2021.

[2] G. Kou, Ö. Olgu Akdeniz, H. Dinçer, and S. Yüksel, "Fintech investments in European banks: a hybrid IT2 fuzzy multidimensional decision-making approach," *Financial Innovation*, vol. 7, no. 1, pp. 39–28, 2021.

[3] Twi Global (n.d.), https://www.twi-global.com/technical-knowledge/faqs/directed- energy-deposition, 2021.

[4] Autonomous Manufacturing, "Metal 3D printing: what is directed energy deposition?," 2018, https://amfg.ai/2018/09/27/metal-3d-printing-what-is-directed-energy- deposition/.

[5] A. Dass and A. Moridi, "State of the art in directed energy deposition: from additive manufacturing to materials design," *Coatings*, vol. 9, no. 7, p. 418, 2019.

[6] M. Ramesh and K. Niranjana, "Effect of process parameters on fused filament fabrication printed composite materials," in *High-Performance Composite Structures*, pp. 155–178, Springer, Singapore, 2022.

[7] M. Ramesh, L. Rajeshkumar, and D. Balaji, "Influence of process parameters on the properties of additively manufactured fiber-reinforced polymer composite materials: a review," *Journal of Materials Engineering and Performance*, vol. 30, no. 7, pp. 4792–4807, 2021.

[8] Additive Manufacturing Research Group, "Loughborough university," https://www.lboro.ac.uk/research/amrg/about/the7categoriesofadditivemanufacturing/directedenergydeposition/.

[9] X. Lu, X. Lin, M. Chiumenti et al., "Residual stress and distortion of rectangular and S-shaped Ti-6Al-4V parts by Directed Energy Deposition: modelling and experimental calibration," *Additive Manufacturing*, vol. 26, pp. 166–179, 2019.

[10] Y. Bandai, "Directed energy deposition (DED), digital alloys' guide to metal additive manufacturing – Part 9," 2019, https://www.digitalalloys.com/blog/directed-energy-deposition/.

[11] J. Ruiz, M. Cortina, J. Arrizubieta, and A. Lamikiz, "Study of the influence of shielding gases on laser metal deposition of Inconel 718 superalloy," *Materials*, vol. 11, no. 8, p. 1388, 2018.

[12] Total Materia, "Introduction to additive manufacturing: Part Two," 2018, https://www.totalmateria.com/page.aspx?ID=CheckArticle&site=ktn&LN=FR&NM= 432.

[13] Engineering product design, "Directed energy deposition (DED)," 2019, https://engineeringproductdesign.com/knowledge-base/directed-energy-deposition/.

[14] Beam Machines, "Ded - directed energy deposition," https://www.beam-machines.com/applications-process-3d-printing.

[15] Sciaky Inc, "What is directed energy deposition (DED) 3D printing? https://www.sciaky.com/additive-manufacturing/what-is-ded-3d-printing.

[16] EWI, "What is directed energy deposition? https://ewi.org/capabilities/additive- manufacturing/what-is-directed-energy-deposition/.

[17] 3D Experience, "3D printing – ADDITIVE, Directed energy deposition - DED, LENS,"https://make.3dexperience.3ds.com/processes/directed-energy- deposition.

[18] S. K. Selvaraj, R. Ramesh, T. M. V. Narendhra et al., "New deveLopments in carbon-based nanomaterials for automotive brake pad applications and future challenges," *Journal of Nanomaterials*, vol. 2021, Article ID 6787435, 24 pages, 2021.

[19] U. Chadha, P. Bhardwaj, R. Agarwal et al., "Recent progress and growth in biosensors technology: a critical review," *Journal of Industrial and Engineering Chemistry*, vol. 109, pp. 21–51, 2022.

[20] A. Tiwari, A. Tiwari, A. Bhatia et al., "Nanomaterials for electromagnetic interference shielding applications: a review," *Nano*, vol. 17, no. 2, Article ID 2230001, 2022.

[21] U. Chadha, P. Bhardwaj, S. K. Selvaraj et al., "Advances in chitosan biopolymer composite materials: from bioengineering, wastewater treatment to agricultural applications," *Materials Research Express*, vol. 9, no. 5, Article ID 052002, 2022.

[22] U. Chadha, S. Sinha, J. Jonna et al., "Review—chemical structures and stability of carbon-doped graphene nanomaterials and the growth temperature of carbon nanomaterials grown by chemical vapor deposition for electrochemical catalysis reactions," *ECS Journal of Solid State Science and Technology*, vol. 11, no. 4, Article ID 041003, 2022.

[23] U. Chadha, S. K. Selvaraj, H. Ashokan et al., "Complex nanomaterials in catalysis for chemically significant applications: from synthesis and hydrocarbon processing to renewable energy applications," *Advances in Materials Science and Engineering*, vol. 2022, Article ID 1552334, 72 pages, 2022.

[24] U. Chadha, S. K. Selvaraj, S. Vishak Thanu et al., "A review of the function of using carbon nanomaterials in membrane filtration for contaminant removal from wastewater," *Materials Research Express*, vol. 9, no. 1, Article ID 012003, 2022.

[25] K. Kulkarni, U. Chadha, S. Yadav et al., "Latest trends and advancement in porous carbon for biowaste organization and utilization," *ECS Journal of Solid State Science and Technology*, vol. 11, no. 1, Article ID 011003, 2022.

[26] S. Yadav, C. P. Paul, A. N. Jinoop, A. K. Rai, and K. S. Bindra, "Laser directed energy deposition based additive manufacturing of copper: process development and material characterizations," *Journal of Manufacturing Processes*, vol. 58, pp. 984–997, 2020.

[27] J. Yu, G. Wang, and Y. Rong, "Experimental study on the surface integrity and chip formation in the micro cutting process," *Procedia Manufacturing*, vol. 1, pp. 655–662, 2015.

[28] Stanford Advanced Materials, "Application of Tungsten in modern industry," https://www.samaterials.com/content/application-of-tungsten-in-modern-industry.html.

[29] W. Jeong, Y. S. Kwon, and D. Kim, "Three-dimensional printing of tungsten structures by directed energy deposition," *Materials and Manufacturing Processes*, vol. 34, no. 9, pp. 986–992, 2019.

[30] V. Madhavadas, D. Srivastava, U. Chadha et al., "A review on metal additive manufacturing for intricately shaped aerospace components," *CIRP Journal of Manufacturing Science and Technology*, vol. 39, no. 2022, pp. 18–36.

[31] A. N. Jinoop, C. P. Paul, and K. S. Bindra, "Laser assisted directed energy deposition of Hastelloy-X," *Optics & Laser Technology*, vol. 109, pp. 14–19, 2019.

[32] F. Careri, S. Imbrogno, D. Umbrello, M. M. Attallah, J. Outeiro, and A. C. Batista, "Machining and heat treatment as post-processing strategies for Ni-superalloys structures fabricated using directed energy deposition," *Journal of Manufacturing Processes*, vol. 61, pp. 236–244, 2021.

[33] T. Bhardwaj, M. Shukla, C. P. Paul, and K. S. Bindra, "Directed energy deposition-laser additive manufacturing of titanium-molybdenum alloy: parametric studies, microstructure and mechanical properties," *Journal of Alloys and Compounds*, vol. 787, pp. 1238–1248, 2019.

[34] A. N. Jinoop, C. P. Paul, and K. S. Bindra, "Laser-assisted directed energy deposition of nickel super alloys: a review," *Proceedings of the Institution of Mechanical Engineers - Part L: Journal of Materials: Design and Applications*, vol. 233, no. 11, pp. 2376–2400, 2019.

[35] Atlantic Steels, "300 series stainless steel," https://www.atlanticstainless.com/steel-grades/300-series-stainless-steel/.

[36] Wikipedia, "Zirconium alloy,".

[37] AlcoTechnics, "Alloy 4043 weld data sheet," http://www.alcotec.com/us/en/support/upload/a4043tds.pdf.

[38] Omnexus, "PMMA or acrylic: guide to support your future "transparent" developments," https://omnexus.specialchem.com/selection-guide/polymethyl-methacrylate-pmma-acrylic-plastic.

[39] O. S. Manoukian, N. Sardashti, T. Stedman et al., "Biomaterials for tissue engineering and regenerative medicine," *Encyclopedia of Biomedical Engineering*, pp. 462–482, 2019.

[40] D. Mitsouras, P. Liacouras, A. Imanzadeh et al., "Medical 3D printing for the radiologist," *RadioGraphics*, vol. 35, no. 7, pp. 1965–1988, 2015.

[41] S. K. Selvaraj, K. Srinivasan, U. Chadha et al., "Contemporary progresses in ultrasonic welding of aluminum metal matrix composites," *Frontiers in Materials*, vol. 8, p. 126, 2021.

[42] Omnexus, "Popular application of polyetheretherketone (PEEK)," https://omnexus.specialchem.com/selection-guide/polyetheretherketone-peek-thermoplastic/key-applications.

[43] M. Rinaldi, F. Cecchini, L. Pigliaru, T. Ghidini, F. Lumaca, and F. Nanni, "Additive manufacturing of polyether ether Ketone (PEEK) for space applications: a nanosat polymeric structure," *Polymers*, vol. 13, no. 1, p. 11, 2020.

[44] Omnexus, "A detailed guide on acrylonitrile Butadiene Styrene," https://omnexus.specialchem.com/selection-guide/acrylonitrile-butadiene-styrene-abs- plastic.

[45] M. Bible, M. Sefa, J. A. Fedchak et al., "3D-Printed acrylonitrile Butadiene styrene-metal organic framework composite materials and their gas storage properties," *3D Printing and Additive Manufacturing*, vol. 5, no. 1, pp. 63–72, 2018.

[46] Omnexus, "The definitive guide to polypropylene (PP)," https://omnexus.specialchem.com/selection-guide/polypropylene-pp-plastic.

[47] W. S. Tan, C. K. Chua, T. H. Chong, A. G. Fane, and A. Jia, "3D printing by selective laser sintering of polypropylene feed channel spacers for spiral wound membrane modules for the water industry," *Virtual and Physical Prototyping*, vol. 11, no. 3, pp. 151–158, 2016.

[48] M. Nofar, D. Sacligil, P. J. Carreau, M. R. Kamal, and M.-C. Heuzey, "Poly (lactic acid) blends: processing, properties and applications," *International Journal of Biological Macromolecules*, vol. 125, pp. 307–360, 2019.

[49] J. Deckers, J. Vleugels, and J.-P. Kruth, "Additive manufacturing of ceramics: a review," *Journal of Ceramic Science and Technology*, vol. 5, 2014.

[50] R. Galante, C. G. Figueiredo-Pina, and A. P. Serro, "Additive manufacturing of ceramics for dental applications: a review," *Dental Materials*, vol. 35, no. 6, pp. 825–846, 2019.

[51] Elan Technology, "96% alumina ceramic," https://www.elantechnology.com/ceramics/ceramic-materials/alumina-ceramics/#:~:text=Alumina%20ceramic%20(Aluminum%20Oxide%20or,resistant%20 to%20wear%20and%20corrosion.&text=Elan%20Technology%20offers%20a%20ran ge,meet%20your%20most%20demanding%20applications.

[52] Superior Technical Ceramics, "Zirconia ceramics," https://www.ceramics.net/ceramic- materials-solutions/zirconia-ceramics.

[53] J. M. Pappas, E. C. Kinzel, and X. Dong, "Laser direct deposited transparent magnesium aluminate spinel ceramics," *Manufacturing Letters*, vol. 24, pp. 92–95, 2020.

[54] D. E. Rumelhart, R. Durbin, R. Golden, and Y. Chauvin, "Backpropagation: the basic theory," *Backpropagation: Theory, architectures and applications*, pp. 1–34, 1995.

[55] F. A. Gers, N. N. Schraudolph, and J. Schmidhuber, "Learning precise timing with LSTM recurrent networks," *Journal of Machine Learning Research*, vol. 3, pp. 115–143, 2002.

[56] Z. Zhang, Z. Liu, and D. Wu, "Prediction of melt pool temperature in directed energy deposition using machine learning," *Additive Manufacturing*, vol. 37, Article ID 101692, 2021.

[57] X. Li, S. Siahpour, J. Lee, Y. Wang, and J. Shi, "Deep learning-based intelligent process monitoring of directed energy deposition in additive manufacturing with thermal images," *Procedia Manufacturing*, vol. 48, pp. 643–649, 2020.

[58] M. Mozaffar, A. Paul, R. Al-Bahrani et al., "Data-driven prediction of the high-dimensional thermal history in directed energy deposition processes via recurrent neural networks," *Manufacturing letters*, vol. 18, pp. 35–39, 2018.

[59] W. Shi, Z. Ren, W. He, J. Hou, H. Xie, and S. Liu, "A technique combining laser spot thermography and neural network for surface crack detection in laser engineered net shaping," *Optics and Lasers in Engineering*, vol. 138, Article ID 106431, 2021.

[60] M. Pant, R. M. Singari, P. K. Arora, G. Moona, and H. Kumar, "Wear assessment of 3–D printed parts of PLA (polylactic acid) using Taguchi design and Artificial Neural Network (ANN) technique," *Materials Research Express*, vol. 7, no. 11, Article ID 115307, 2020.

[61] Z. L. Lu, D. C. Li, B. H. Lu, A. F. Zhang, G. X. Zhu, and G. Pi, "The prediction of the building precision in the Laser Engineered Net Shaping process using advanced networks," *Optics and Lasers in Engineering*, vol. 48, no. 5, pp. 519–525, 2010.

[62] B. Li, F. Wu, S. N. Lim, S. Belongie, and K. Q. Weinberger, "On feature normalization and data augmentation," in *Proceedings of the IEEE/CVF Conference on Computer Vision and Pattern Recognition*, pp. 12383–12392, Nashville, TN, USA, June 2021.

[63] B. Bhattacherjee, S. Mukherjee, and R. Sengupta, "Study of energy deposition patterns in hadron calorimeter for prompt

and displaced jets using convolutional neural network," *Journal of High Energy Physics*, vol. 2019, no. 11, pp. 156–232, 2019.

[64] Y. Sun, W. Zeng, Y. Han et al., "Modeling the correlation between microstructure and the properties of the Ti–6Al–4V alloy based on an artificial neural network," *Materials Science and Engineering: A*, vol. 528, no. 29-30, pp. 8757–8764, 2011.

[65] B. J. Hayes, B. W. Martin, B. Welk et al., "Predicting tensile properties of Ti-6Al-4V produced via directed energy deposition," *Acta Materialia*, vol. 133, pp. 120–133, 2017.

[66] M. Juhasz, "Machine learning predictions of single clad geometry in directed energy deposition," *OSF Preprints - Open Science Framewor*, 2020.

[67] L. Yu, R. Zhou, R. Chen, and K. K. Lai, "Missing data preprocessing in credit classification: one-hot encoding or imputation?" *Emerging Markets Finance and Trade*, vol. 58, no. 2, pp. 472–482, 2022.

[68] J. Yamanaka, S. Kuwashima, and T. Kurita, "Fast and accurate image super resolution by deep CNN with skip connection and network in network," in *Proceedings of the International Conference on Neural Information Processing*, pp. 217–225, Springer, Bangkok, Thailand, November 2017.

[69] S. Prakash and S. Suman, "Neural network-based prediction for surface characteristics in CO 2 laser micro-milling of glass fiber reinforced plastic composite," *Neural Computing & Applications*, vol. 33, no. 18, pp. 11517–11529, 2021.

[70] J. Li, M. Sage, X. Guan, M. Brochu, and Y. F. Zhao, "Machine learning- enabled competitive grain growth behavior study in directed energy deposition fabricated Ti6Al4V," *Journal of Occupational Medicine*, vol. 72, no. 1, pp. 458–464, 2020.

[71] A. Syuhada, M. S. Shamsudin, M. F. Omar, S. K. Ghoshal, S. W. Harun, and M. S. Aziz, "Incorporating 3D metal printing with artificial intelligence in meeting aerospace demands," in *Journal of Physics: Conference Series*vol. 1892, no. 1, IOP Publishing, Article ID 012015, 2021.

[72] V. Gribova, Y. Kulchin, A. Nikitin, and V. Timchenko, "The concept of support for laser-based additive manufacturing on the basis of artificial intelligence methods," in *Russian Conference on Artificial Intelligence*, pp. 403–415, Springer, Berlin, Germany, 2020.

[73] J. C. Heigel, P. Michaleris, and E. W. Reutzel, "Thermomechanical model development and validation of directed energy deposition additive manufacturing of Ti–6Al–4V," *Additive Manufacturing*, vol. 5, pp. 9–19, 2015.

[74] Q. Yang, P. Zhang, L. Cheng, Z. Min, M. Chyu, and A. C. To, "Finite element modeling and validation of thermomechanical behavior of Ti-6Al-4V in directed energy deposition additive manufacturing," *Additive Manufacturing*, vol. 12, pp. 169–177, 2016.

[75] Y. Huang, M. Ansari, H. Asgari et al., "Rapid prediction of real-time thermal characteristics, solidification parameters and microstructure in laser directed energy deposition (powder-fed additive manufacturing)," *Journal of Materials Processing Technology*, vol. 274, Article ID 116286, 2019.

[76] J. Xu, X. Gu, D. Ding, Z. Pan, and K. Chen, "A review of slicing methods for directed energy deposition based additive manufacturing," *Rapid Prototyping Journal*, vol. 24, no. 6, pp. 1012–1025, 2018.

[77] S. J. Wolff, H. Wu, N. Parab et al., "In-situ high-speed X-ray imaging of piezo-driven directed energy deposition additive manufacturing," *Scientific Reports*, vol. 9, no. 1, p. 962, 2019.

[78] H.-W. Hsu, Y.-L. Lo, and M.-H. Lee, "Vision-based inspection system for cladding height measurement in directed energy deposition (DED)," *Additive Manufacturing*, vol. 27, pp. 372–378, 2019.

[79] S. M. Thompson, L. Bian, N. Shamsaei, and A. Yadollahi, "An overview of Direct Laser Deposition for additive manufacturing; Part I: transport phenomena, modeling, and diagnostics," *Additive Manufacturing*, vol. 8, pp. 36–62, 2015.

[80] M. Javidani, J. Arreguin-Zavala, J. Danovitch, Y. Tian, and M. Brochu, "Additive manufacturing of AlSi10Mg alloy using directed energy deposition: microstructure and hardness characterization," *Journal of Thermal Spray Technology*, vol. 26, no. 4, pp. 587–597, 2016.

[81] A. N. Jinoop, C. P. Paul, S. K. Mishra, and K. S. Bindra, "Laser Additive Manufacturing using directed energy deposition of Inconel-718 wall structures with tailored characteristics," *Vacuum*, vol. 166, pp. 270–278, 2019.

[82] A. Saboori, A. Aversa, G. Marchese, S. Biamino, M. Lombardi, and P. Fino, "Microstructure and mechanical properties of AISI 316L produced by directed energy deposition-based additive manufacturing: a review," *Applied Sciences*, vol. 10, no. 9, p. 3310, 2020.

[83] A. Saboori, D. Gallo, S. Biamino, P. Fino, and M. Lombardi, "An overview of additive manufacturing of titanium components by directed energy deposition: microstructure and mechanical properties," *Applied Sciences*, vol. 7, no. 9, p. 883, 2017.

[84] M. A. Melia, H.-D. A. Nguyen, J. M. Rodelas, and E. J. Schindelholz, "Corrosion properties of 304L stainless steel made by directed energy deposition additive manufacturing," *Corrosion Science*, vol. 152.

[85] J. S. Park, M.-G. Lee, Y.-J. Cho et al., "Effect of heat treatment on the characteristics of tool steel deposited by the directed energy deposition process," *Metals and Materials International*, vol. 22, no. 1, pp. 143–147, 2016.

[86] A. Fiorese, "The advantages of heat treating metals following additive manufacturing," 2020, https://www.industrialheating.com/articles/95878-the-advantages-of-heat-treating-metals-following-additive-manufacturing.

[87] I. Gibson, D. Rosen, and B. Stucker, "Directed energy deposition processes," *Additive Manufacturing Technologies*, Springer, Berlin, Germany, pp. 245–268, 2015.

[88] D.-S. Shim, G.-Y. Baek, J.-S. Seo, G.-Y. Shin, K.-P. Kim, and K.-Y. Lee, "Effect of layer thickness setting on deposition characteristics in directed energy deposition (DED) process," *Optics & Laser Technology*, vol. 86, pp. 69–78, 2016.

[89] D. R. Feenstra, A. Molotnikov, and N. Birbilis, "Utilisation of artificial neural networks to rationalise processing windows in directed energy deposition applications," *Materials & Design*, vol. 198, 2021.

[90] R. M. Mahamood, "Effect of laser power and gas flow rate on properties of directed energy deposition of titanium alloy," *Lasers in Manufacturing and Materials Processing*, vol. 5, no. 1, pp. 42–52, 2018.

[91] R. Parekh, R. K. Buddu, and R. I. Patel, "Multiphysics simulation of laser cladding process to study the effect of process parameters on clad geometry," *Procedia Technology*, vol. 23, pp. 529–536, 2016.

[92] L. Tang, J. Ruan, R. G. Landers, and F. Liou, "Variable powder flow rate control in laser metal deposition processes," *Journal of Manufacturing Science and Engineering*, vol. 130, no. 4, Article ID 041016, 2008.

[93] Y. Huang, D. Wu, D. Zhao et al., "Process optimization of melt growth alumina/aluminum titanate composites directed energy deposition: effects of scanning speed," *Additive Manufacturing*, vol. 35, Article ID 101210, 2020.

[94] T. Bhardwaj and M. Shukla, "Laser additive manufacturing-directed energy deposition of Ti-15Mo biomedical alloy: artificial neural network based modeling of track dilution," *Lasers in Manufacturing and Materials Processing*, vol. 7, no. 3, pp. 245–258, 2020.

[95] R. Sivasubramani, A. Verma, G. Rithvik, U. Chadha, and S. Senthil Kumaran, "Influence on nonhomogeneous microstructure formation and its role on tensile and fatigue performance of duplex stainless steel by a solid-state welding process," *Materials Today Proceedings*, vol. 46, pp. 7284–7296, 2021.

[96] A. Sharma, A. Chouhan, L. Pavithran, U. Chadha, and S. K. Selvaraj, "Implementation of LSS framework in automotive component manufacturing: a review, current scenario, and future directions," *Materials Today Proceedings*, vol. 46, pp. 7815–7824, 2021.

[97] A. Raj, S. Ram Kishore, L. Jose, A. K. Karn, U. Chadha, and S. K. Selvaraj, "A survey of electromagnetic metal casting computation designs, present approaches, future possibilities, and practical issues," *The European Physical Journal Plus*, vol. 136, no. 6, pp. 704–733, 2021.

[98] K. Virmani, C. Deepak, S. Sharma, U. Chadha, and S. K. Selvaraj, "Nanomaterials for automotive outer panel components: a review," *The European Physical Journal Plus*, vol. 136, no. 9, pp. 921–929, 2021.

[99] T. Ghimire, A. Joshi, S. Sen, C. Kapruan, U. Chadha, and S. K. Selvaraj, "Blockchain in additive manufacturing processes: recent trends & its future possibilities," *Materials Today Proceedings*, vol. 50, pp. 2170–2180, 2022.

[100] T. Pati, S. Kabra, and U. Chadha, "Statistical quality study of the parts produced in an automobile industry: a daimler India case study," *IOP Conference Series: Materials Science and Engineering*, IOP Publishing, vol. 1206, no. 1, , Article ID 012022, 2021.

[101] M. Dharnidharka, U. Chadha, L. M. Dasari, A. Paliwal, Y. Surya, and S. K. Selvaraj, "Optical tomography in additive manufacturing: a review, processes, open problems, and new opportunities," *The European Physical Journal Plus*, vol. 136, no. 11, pp. 1133–1228, 2021.

[102] S. K. Selvaraj, A. Raj, M. Dharnidharka et al., "A cutting-edge survey of tribological behavior evaluation using artificial and computational intelligence models," *Advances in Materials Science and Engineering*, vol. 2021, Article ID 9529199, 17 pages, 2021.

[103] S. K. Selvaraj, A. Raj, R. Rishikesh Mahadevan, U. Chadha, and V. Paramasivam, "A review on machine learning models in injection molding machines," *Advances in Materials Science and Engineering*, vol. 2022, Article ID 1949061, 28 pages, 2022.

[104] U. Chadha, A. Abrol, N. P. Vora, A. Tiwari, S. K. Shanker, and S. K. Selvaraj, "Performance evaluation of 3D printing technologies: a review, recent advances, current challenges, and future directions," *Progress in Additive Manufacturing*, 2022, In press.

[105] U. Chadha, S. K. Selvaraj, H. Pant et al., "Phase change materials in metal casting processes: a critical review, and future possibilities," *Advances in Materials Science and Engineering*, vol. 2022, Article ID 7520308, 14 pages, 2022.

[106] U. Chadha, S. K. Selvaraj, A. K. Ravinuthala et al., "Bio-inspired techniques in freeze casting: a survey of processes, current advances, and future directions," *International Journal of Polymer Science*, vol. 2022, Article ID 9169046, 22 pages, 2022.

[107] A. Adefris, D. Desalegn, S. K. Selvaraj, V. Paramasivam, and U. Chadha, "Experimental investigation of sorghum stalk and sugarcane bagasse hybrid composite for particleboard," *Advances in Materials Science and Engineering*, vol. 2022, Article ID 1844004, 17 pages, 2022.

[108] T. Pereira, J. V. Kennedy, and J. Potgieter, "A comparison of traditional manufacturing vs additive manufacturing, the best method for the job," *Procedia Manufacturing*, vol. 30, pp. 11–18, 2019.

[109] M. Attaran, "The rise of 3-D printing: the advantages of additive manufacturing over traditional manufacturing," *Business Horizons*, vol. 60, no. 5, pp. 677–688, 2017.

[110] A. Ge, "What is additive manufacturing? https://www.ge.com/additive/additive-manufacturing.

[111] K. Stevenson, "How could additive manufacturing replace traditional manufacturing?," 2020, https://www.fabbaloo.com/news/how-could-additive-manufacturing-replace-traditional-manufacturing.

[112] American Manufacturing, "3D printing vs traditional manufacturing," 2015, https://www.marlinwire.com/blog/3d-printing-vs-traditional-manufacturing.

[113] S. Hochreiter, "The vanishing gradient problem during learning recurrent neural nets and problem solutions," *International Journal of Uncertainty, Fuzziness and Knowledge-Based Systems*, vol. 6, no. 2, pp. 107–116, 1998.

[114] U. Chadha, S. K. Selvaraj, N. Gunreddy et al., "A survey of machine learning in friction stir welding, including unresolved issues and future research directions," *Material Design & Processing Communications*, vol. 2022, Article ID 2568347, 28 pages, 2022.

[115] U. Chadha, S. K. Selvaraj, A. Raj et al., "AI-driven techniques for controlling the metal melting production: a review, processes, enabling technologies, solutions, and research challenges," *Materials Research Express*, vol. 9, no. 7, Article ID 072001, 2022.

[116] I. Sachdeva, S. Ramesh, U. Chadha, H. Punugoti, and S. Kumaran Selvaraj, "Computational AI models in VAT photopolymerization: a review, current trends, open issues, and future opportunities," in *Neural Computing and Applications*, Springer, Berlin, Germany, 2022.